STUDY OF SANDY SLOPES THROUGH SMALL-SCALE PHYSICAL MODELING

by

Cemal Can Ansen

B.S., Civil Engineering, Middle East Technical University, 2018

Submitted to the Institute for Graduate Studies in
Science and Engineering in partial fulfillment of
the requirements for the degree of
Master of Science

Graduate Program in Civil Engineering

Boğaziçi University

2025

ACKNOWLEDGEMENTS

I wish to express my sincere gratitude to my advisor, Assistant Professor İrem Zeynep Yıldırım, for her insightful guidance, unwavering support, and encouragement throughout this research. Her expertise and dedication have been crucial to the development and completion of this thesis.

Also, I thank Emre Tekdemir for his invaluable assistance during the numerical stages of this study and contributions to the structuring of the process. I am also indebted to my friend Muhammed Ömer Canbulat, who almost never left me alone throughout the laboratory experiments. I am deeply grateful to my family and friends for their support throughout this journey.

Lastly, I acknowledge the financial support provided by Boğaziçi University Scientific Research Projects Fund with Grant Number 19855.

ABSTRACT

STUDY OF SANDY SLOPES THROUGH SMALL-SCALE PHYSICAL MODELING

This research study integrates experimental studies on small-scale physical model tests with finite element analysis to investigate the behavior of locally loaded sandy slopes and locally loaded sandy slopes stabilized with piles. The primary objective of this study was to develop an experimental setup for small-scale physical models, replicating the behavior of full-scale locally loaded sandy slopes. Initially, a series of tests was conducted on the sand selected for the model test to assess its index and strength parameters. Then, density calibration tests were performed on the pluviation setup to examine the effects of valve opening and drop height on the relative density of the sand. The sand was placed in the model tank at the desired density, and a series of tests were carried out on the small-scale (1/40) physical slope model. Local loads were exerted on the sandy slope models using a displacement-controlled loading system. The slope failure shapes were observed by taking continuous images of the slope from the top and one side of the model tank. Tests were conducted on slopes with sand prepared at 40% (medium dense) and 70% (dense) relative density values. The piles were modeled using hollow polyvinyl chloride pipes. The mechanics of a stabilized sandy slope were investigated, with a particular focus on the role of pile stabilization in enhancing the arching mechanism, improving load distribution and slope stability, and reducing displacements. For validation purposes, the experimental results from the physical model tests were compared with the numerical analysis results of the physical model, obtained using the three-dimensional finite element method. The results of this study showed that the behavior of the newly developed small-scale physical slope model was similar to that obtained from the numerical analysis. The dense sandy slope model exhibited a stiffer (steeper) initial curve for the vertical displacement versus vertical stress response compared to the medium-dense sandy slope model. For the same vertical displacement, pile stabilization significantly improved the vertical stress response of the of the locally loaded slope constructed with medium dense sand. The results of the numerical analysis showed a load response behavior similar to that observed in the experimental results. The differences observed between the experimental and numerical results were primarily attributed to the limitations of small-scale tests.

ÖZET

KÜÇÜK ÖLÇEKLİ FİZİKSEL MODELLEME İLE KUMLU ŞEVLERİN İNCELENMESİ

Bu araştırmada, küçük ölçekli fiziksel model deneyleri ve sonlu elemanlar analizi kullanılarak, lokal yükler altındaki kumlu şevlerin ve kazıklarla stabilize edilmiş kumlu şevlerin davranışı incelenmiştir. Bu çalışmanın temel amacı, lokal yük altındaki kumlu şevlerin davranışını inceleyebilmek için küçük ölçekli bir deney düzeneği geliştirmektir. Öncelikle, model testlerinde kullanılan kumun indeks özelliklerini ve mukavemet parametrelerini değerlendirmek için bir dizi test gerçekleştirilmiştir. Araştırma kapsamında ilk olarak, model tankında kullanılacak kumun indeks ve dayanım parametrelerini belirlemek için deneyler yapılmıştır. Daha sonra, yağmurlama düzeneğinde yapılan kalibrasyon testleri ile vana açıklığının ve düşme yüksekliğinin kumun rölatif sıkılığı üzerindeki etkileri incelenmiştir. Kum, model tankına istenilen sıkılıklarda yerleştirilmiş ve küçük ölçekli (1/40) fiziksel şev modeli modelleri üzerinde deneyler yapılmıştır. Deplasman kontrollü bir yükleme sistemi aracılığıyla kumlu şev modellerine lokal yüklemeler uygulanmıştır. Şevin göçme şekilleri, model tankının üstünden ve yanından sürekli görüntüler alınarak takip edilmiştir. Testler %40 (orta derecede sıkı) ve %70 rölatif sıklıkta kum şevlerde gerçekleştirilmiştir. Kazıklar, içi boş polivinil klorür (PVC) borular kullanılarak modellenmiştir. Kazık ile stabilize edilmiş kumlu şevlerin davranışı incelenmiş ve kazık stabilizasyonun kemerleme mekanizmasını geliştirme, yük dağılımını iyileştirme, şev stabilitesini artırma ve yer değiştirmeleri azaltmadaki rolü araştırılmıştır. Fiziksel model deneylerinden elde edilen sonuçlar, doğrulama amacıyla üç boyutlu sonlu elemanlar yöntemiyle yapılan sayısal analiz sonuçlarıyla karşılaştırılmıştır. Çalışmanın bulguları, küçük ölçekli fiziksel şev modelinin genel olarak sayısal analizlerle uyumlu bir davranış sergilediğini göstermektedir. Sıkı kumlu şev modelinin, orta sıkılıkta kumlu şev modeline kıyasla, düşey deplasman - düşey gerilme grafiğinde başlangıçta daha dik (daha sert) bir eğriye sahip olduğu belirlenmiştir. Aynı düşey deplasman seviyesinde, kazık stabilizasyonun lokal yük altındaki orta sıkılıktaki kumlu şevin düşey gerilmesini önemli ölçüde iyileştirdiği gözlenmiştir. Sayısal analiz sonuçlarının, yükleme tepkisi açısından deney sonuçlarına benzediği görülmüştür. Deney ve sayısal sonuçlar arasındaki farklılıklar, testlerin küçük ölçekli olmasıyla ilişkilendirilmiştir.

TABLE OF CONTENTS

LIST OF FIGURES

LIST OF TABLES

LIST OF SYMBOLS

d_{50}	Mean grain size of soil
d_p	Pile diameter
E_{50}^{ref}	Secant stiffness in standard drained triaxial test
E_{oed}^{ref}	Tangent stiffness for primary oedometer loading
E_p	Modulus of elasticity of pile
E_{ur}^{ref}	Unloading/ reloading stiffness
G_s	Specific gravity
Ip	Stiffness of pile
k	Subgrade reaction modulus
L_p	Length of pile
m	Power for stress level dependency of stiffness
p^{ref}	Reference pressure
v	Poisson ratio
v_{ur}	Poisson's ratio for unloading – reloading
γ_d	Dry unit weight
λ	Scale factor
ϕ	Friction angle
ψ	Dilatancy angle

LIST OF ACRONYMS / ABBREVIATONS

3D	Three-dimensional
1-g	Single gravity
D_R	Relative density of soil
FE	Finite Element
FEM	Finite Element Method
F_s	Factor of Safety
HS	Hardening Soil
PC	Polycarbonate
PIV	Particle Image Velocity
PVC	Polyvinyl Chloride

1. INTRODUCTION

1.1. General

Slope stability is a fundamental concern in geotechnical engineering, as slope failures can cause significant damage to infrastructure and the environment and may even result in loss of human life. The increasing demand for cost-effective and reliable slope stabilization methods has driven the development of various techniques, including the installation of reinforcing or stabilizing elements. These elements can be inclusions of steel strips or geosynthetics in man-made slopes. In natural slopes, the inclusion of layered reinforcement elements is not feasible, and piles are commonly installed for stabilization and reinforcement purposes. The design for slope stabilization requires understanding the interactions between soil and these reinforcement elements. Understanding these interactions becomes particularly important when designing slopes that are expected to withstand static and dynamic loads.

Loaded slopes and loaded slopes stabilized with piles, can be investigated using both laboratory models and numerical simulations. Physical models, particularly at small scales, allow researchers to replicate and observe slope-load and slope-reinforcement interaction mechanisms, as well as slope failure, in a controlled setting. Even at small scales, development of physical model tests requires major human effort and time. Numerical modeling, on the other hand, helps the researchers to analyze numerous cases rather quickly. Numerical analysis can be a useful tool to better understand the experimental observations and to assess the shortcomings of the experimental setup if any. It is also important to note that numerical modeling is the only powerful technique to capture real field conditions, as physical models cannot be easily built for complex geologies and slope geometries. When combined, physical modeling and numerical analysis provide a deeper understanding of slopes and stabilization methods. Their use together is also required for validation purposes.

In this study, a sustainable small-scale model test experimental setup was developed to comprehend the behavior of locally loaded slopes stabilized with piles. The research work also integrated experimental studies on small-scale physical model tests with finite element (FE) analysis to understand the behavior of locally loaded sandy slopes and local-loaded sandy slopes stabilized using piles. This combined approach is instrumental in understanding the effects of various parameters on the behavior of locally loaded slopes stabilized with piles.

1.2. Objective and Scope of Study

This study aimed to study the behavior of locally loaded sandy slopes and slopes stabilized with piles using both experimental studies and numerical analysis for validation purposes. The primary objective of this thesis was to develop a reliable experimental setup for a small-scale physical model that replicates the behavior of full-scale, locally loaded sandy slopes. Additionally, installation of stabilization piles was also included in the physical model. The behavior of locally loaded pile-stabilized slopes were also investigated through small-scale physical model tests. After the development of the experimental setup, special attention was given to controlling and calibrating critical parameters, such as the relative density (D_R) of the sand in the model tank. Several calibration tests were also performed to observe the reliability of the setup and measurement systems. The effect of D_R on the stability of a locally loaded sandy slope was investigated. The mechanics of a stabilized sandy slope were explored through observations, with a particular focus on the role of pile stabilization in enhancing the arching mechanism, load distribution, slope stability, and reducing the displacements.

The small-scale test setups were also modeled using numerical simulations for comparison purposes. Three-dimensional (3D) finite element modeling (FEM) was employed for numerical analysis, which involved careful definition of material properties, model configurations, and construction stages to accurately replicate the experimental conditions. The results of the small-scale physical model tests were compared with those obtained from the numerical analysis performed using 3D FEM.

1.3. Thesis Organization

This research thesis is organized into six (6) main chapters. Chapter 1 is the introduction, providing a general overview, objectives, and scope of the research. Chapter 2 reviews the literature on slope stability, focusing on slope failure mechanisms, physical modeling techniques, and previous studies on small-scale tests on slopes and slopes stabilized with piles. Chapter 3 explains the development of the small-scale physical model experimental setup and the results of the calibration studies. Additionally, the results of the laboratory tests performed on the sand used in the slope model, the density calibration tests performed in the model test box, instrumentation details, and imaging techniques are also provided in this Chapter. Chapter 4 presents the results of the small-scale physical model tests performed on locally loaded sandy slopes and stabilized slopes. The effects of D_R and stabilization with piles were discussed based on test results. Chapter 5 presents the numerical analysis approach using 3D FEM in Plaxis 3D. The results of the numerical analysis simulating the models of locally loaded slopes and those stabilized with piles were compared with the experimental findings from small-scale physical model tests. Finally, Chapter 6 summarizes the research findings, highlights the study's contributions, and suggests directions for future work.

2. LITERATURE REVIEW

This chapter presents a literature review on various aspects of slope stability, focusing on how the slope and stabilization can be represented in a controlled laboratory environment, focusing on by using piles for stabilization. At the beginning of this chapter, an overview of slope stability and its fundamental concepts is provided along with a brief definition of slope stabilization methods. Afterwards, laboratory model tests, performed on slopes and pile-stabilized slopes from the literature are presented. Based on previous research, the literature was specifically investigated to assess soil materials, scaling methods, scale factors, pile material and dimensions, and loading rates utilized in the model tests. A summary of the literature review was provided. The Chapter concludes with measurement techniques and data acquisition systems used in the model tests presented in the literature.

2.1. Overview of Slope Failures and Stability Solutions

Slopes, whether natural or artificial, shape the topography of landscapes and impact the stability of structures located nearby them. Natural slopes are formed through natural processes such as erosion and weathering. Artificial slopes, on the other hand, are generally constructed embankments and cut slopes created by humans. Both types of slopes require careful design and continuous monitoring to ensure stability and minimize risks associated with failures. To ensure the stability of slopes, it is important to understand possible types of failures. Different failure types have been observed, including rotational slips, translational slips, and compound slips, each associated with different soil conditions and slope geometries. Figure 2.1 shows an illustration of the typical slope failures presented by Craig (2004).

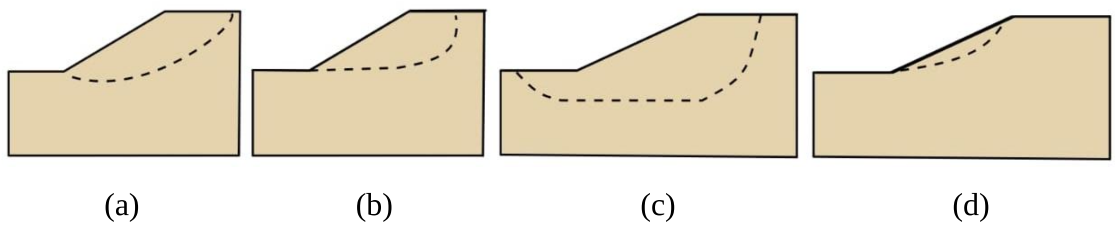

Figure 2.1. Illustration of typical slope failure mechanism: a) circular, b) non-circular, c) compound slip, d) translation slip (modified after Craig 2004).

To analyze slopes, various methods have been proposed in the literature. One of the most common ones is the limit equilibrium method. The limit equilibrium method assumes that failure occurs along a preknown failure surface. There are various limit equilibrium methods, some of which assume a single body where whereas others, known as “slice methods,” divide the slope into trapezoidal slices. The forces and moments acting on each slice are calculated, and equilibrium conditions are checked to evaluate slope stability (Craig, 2004). Common approaches within this method include Bishop's Method, Janbu Method, and Spencer's Method. Another widely used approach is deformation analysis, often conducted through either finite difference or finite element methods. With these methods, stress distribution and deformations, as well as movements, and pore pressures in soil masses, slopes and embankments can be evaluated (Duncan, 1996).

There are various slope stabilization techniques. One of them includes the installation of reinforcing or stabilizing elements. These elements can be inclusions of steel strips or geosynthetics in man-made slopes. Furthermore, strategic interventions in the form of effective drainage solutions and the implementation of retention structures, such as retaining walls, also offer proactive stabilization by removing water-induced pressures and/or providing lateral support. One of the widely used slope stabilization methods is the implementation of drilled shafts or driven piles to increase the resisting forces against sliding forces. This method is very commonly applied in highway cuts and stabilizing preexisting natural slopes in which inclusion of other reinforcing elements such as geosynthetics is not possible.

Although numerical analysis provides rather fast and practical solutions, physical modeling has unique advantages. It offers the opportunity to observe the progressive failure mechanisms and effectiveness of slope stabilization techniques in the laboratory environment. Validation of numerical analysis can only be possible through physical model tests. Real-scale physical modeling eliminates major issues caused by scaling effects, but they are not always feasible due to cost and space limitations. One of the options can be reducing the size of the model. This simplifies the problem and reduces costs, making it more convenient to analyze geotechnical problems. However, small-scale physical models have shortcomings, particularly in realistically representing in-situ stresses and achieving complete compliance with scaling methods.

2.2. Physical Modeling Methods

Physical modeling serves to reduce the size of a large structure, such as a slope, building, or pile, known as the "prototype." The relationship between the prototype and the model is governed by analytical expressions that show the correlation between their relevant geometrical and physical parameters due to size reduction. These expressions are commonly based on principles of similarity and similitude laws. The similarity ratio between the prototype and the model is generally defined by scale factors. For a given model test, scale factors are different for quantities such as length, density and strength (Iai 1989). There are two (2) main types of scale-model tests based on the generation of the stress field: *(i)* ng – with a centrifugal force applied using a centrifuge test machine and *(ii)* 1-g – under normal gravity condition.

In centrifuge tests, a physical model is rotated inside a centrifuge machine. This rotational motion induces centripetal acceleration, effectively magnifying the local gravitational forces acting on the model. Consequently, the resulting stresses experienced by the model replicate the conditions it would encounter if it were at the same scale as the prototype. If the tests are performed without centripetal acceleration, then the Earth's gravitational acceleration is used as a reference, and accordingly, the term "1-g" physical model tests refers to these physical model tests performed without centrifugal force.

Small-scale physical model tests performed under 1-g conditions are significantly less expensive than full-scale tests or centrifuge tests. By using smaller models, researchers conserve physical resources and significantly reduce testing costs.

2.3. Reduced Scale 1-g Model Tests on Slopes and Stabilized Slopes

In order to ensure the reliability and repeatability of physical model tests, careful preparation of the model and its are crucial steps. The design and construction of physical models involve several essential steps, including determining the objectives, selecting the appropriate scale factors, choosing suitable materials, and instrumenting the model with sensors and measurement devices (Al Heib et al. 2020). The correlations between prototype-scale and model-scale parameters are defined by analytical expressions that incorporate a simple size reduction scale factor, which is generally defined as the geometric scale factor.

Iai (1989) suggested the use of three (3) main scale factors for various parameters in geotechnical modeling: (*i*) geometric scale factor, (*ii*) soil density factor, and (*iii*) soil strain factor. The geometric scale factor (n) is defined as the ratio of the dimensions of the prototype to those of the physical model. Geometric scale is used to maintain the geometric similarity between the model and the prototype. The soil density scale factor represents the ratio of the soil density of the prototype to the soil density of the model. It is important to note that the actual density of the soil is also related to its particle size. This means that ideally, the particle size of the soil must also be scaled in physical model tests, when the density of the soil is in discussion. However, it is a real challenge to use scaled particles in physical models, and hence this aspect is commonly ignored. Therefore, in geotechnical models that use any type of soil or granular material, it is common to assume a density scale factor of 1. This means that the density of the soil in the models is generally kept as the same as the prototype. Soil strain scale factor represents the scaling of the soil deformations (*i.e.,* strains) in the model compared to the prototype. The value of the soil strain scale factor typically ranges between 1 and the geometric scale factor (n), indicating the level of strain that is scaled in the model.

Wood et al.(2002) compiled research studies, including those by Sabnis et al. (1983), Krawinkler (1979), Iai (1989), and Schofield and Steedman (1988), that use scaling factors in geotechnical models. He emphasizes the importance of considering stiffness in scaling, that is often overlooked even when strains are considered. He suggested that it is beneficial to treat stiffness as an independent scale factor rather than solely relying on strain considerations. Wood et al. (2002) suggested that four (4) main scale factors should be considered in geotechnical model tests under: *(i)* ng and *(ii)* 1-g –gravity conditions. These are length, density, stiffness, and acceleration. The scale factors for other parameters (*i.e.*, stress, strain, displacement and pile flexural rigidity) can be derived from these main scale factors. The scaling factors and the corresponding lengths in the single gravity (1-g) models, suggested by Wood et al. (2002) are presented in Table 2.1. The "α" used as the exponent in the scale factor relationships is selected based on soil type. As an example, α is taken as 0.5 for sand-like soils and 1 for clayey soils (Wood et al., 2002). The sand behavior is a function of both the stress state and initial void ratio. Therefore, it is necessary to work with a higher void ratio to replicate the desired behavior observed in the prototype (Altaee and Fellenius 1994; Bhattacharya et al. 2011).

Table 2.1. Physical model tests scale factors (Wood et al., 2002).

Variable	Symbols of scale factors (model/prototype)	Corresponding length in 1-g model
Length (geometric)	n_l	1/n
density	n_p	1
stiffness	n_g	$1/n^{\alpha}$
acceleration	n_G	1
stress	$n_p n_g n_l$	1/n
strain	$n_p n_g n_l / n_G$	$1/(n^{1-\alpha})$
displacement	$n_p n_g n_l^2 / n_G$	$1/(n^{2-\alpha})$
pile flexural rigidity	$n_G n_l^4$	$1/(n^{4+\alpha})$

Note: n =geometric scale factor= ratio of the dimensions of the prototype to those of the model.

2.4. Physical Model Tests Under Static Load

Several researchers investigated different aspects of the slopes and slopes stabilized piles using physical model tests (Kahyaoglu 2010, Rathod et al. 2019, Mazaheri et al. 2021).

Generally, these tests were performed to investigate deformations on the slope and strains in the piles. Majority of the model tests were performed in sand, however a few researchers utilized clay (Rathod et al. 2019, Ozkahriman and Wartman 2007) and gravels (Fu et al. 2019).

Ozkahriman and Wartman (2007), conducted a study that focus on cohesive model slopes and their behavior under static conditions. Three (3) small-scale physical model slopes were tested with different geometric scaling factors. The models used artificial, fully saturated clay consisting of a mixture of kaolinite and bentonite. In the tests, displacement potentiometers were strategically placed along the slope and at the crest to measure the deformation response of the model. Accelerometers were also positioned near the back of the model to measure the shear wave velocity of the soft clay before testing. A surface load was applied using a Plexiglas " with a thickness of 1.90 cm that represents a footing, and the load was measured using a load cell. A simple sketch of their experimental setup and instrumentation details is provided in Figure 2.2. Using a geometric scaling factor (n) of 22, the model represents a 12 m high soft clay embankment with a 45˚ slope. The soft clay had an undrained shear strength of 75 kPa and the shear wave velocity was measured as 45 m/s in clay. The scaling factors proposed by Iai (1989) for 1-g physical modeling were utilized in this study. The results of three (3) different scaled models exhibited a generally consistent response indicated that fully saturated cohesive soils under undrained conditions can be simulated with appropriate scale factors. Specifically, differences emerged in the ultimate capacity and the failure surface between models were attributed to the boundary effects.

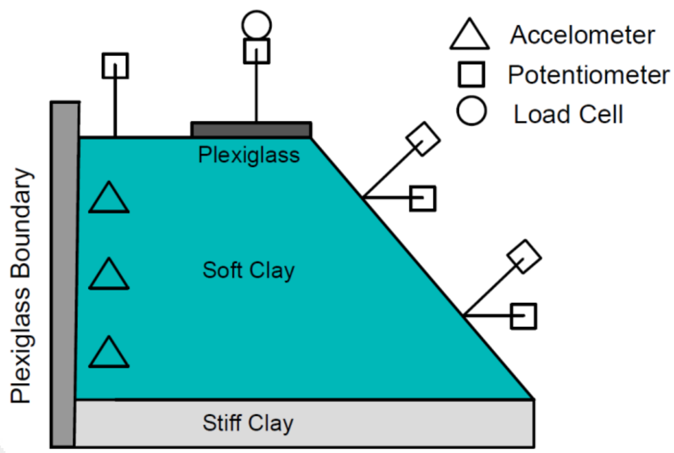

Figure 2.2. Experimental set up and instrumentation plan of locally loaded slope (modified after Ozkahriman and Wartman, 2007).

Madhumathi and Ilamparuthi (2018), focused on determining the behavior and load-carrying capacity of individual piles responding to soil movement caused by an excavation that generates a slope. An illustration of the physical model test components of this study is shown in Figure 2.3. This study investigated the response of a single pile to soil movement induced by excavation. The researchers conducted model tests at 1-g, using piles with three (3) different pile length-to-diameter ratios (L_p/d_p ratio) of 10, 20, and 30, embedded in medium dense sand. They observed that the deflection and bending moment of the pile head decreased exponentially as the distance between the pile and the sheet pile wall supporting the excavation increased. For the model tests, the researchers fabricated model piles using the scale method proposed by Wood et al. (2002), with a scale factor of 20. The model piles were made from hollow circular aluminum tubes with a diameter of 19.05 mm. The tests were conducted in a steel tank with dimensions of 1x0.6x1m and clean river sand was used. The results of the physical modeling approach were compared with the numerical simulations of the prototype. The simulated prototype performance was compared with the measured results by converting the model results back to the prototype scale using the scaling factor recommended by Wood et al. (2002). The results obtained from the FE analysis of the prototype agreed well with the results obtained using this scaling method , as well as with the design methods proposed by Chen and Poulos (1997), Xu and Poulos (2001), and the centrifuge results of Leung et al. (2000).

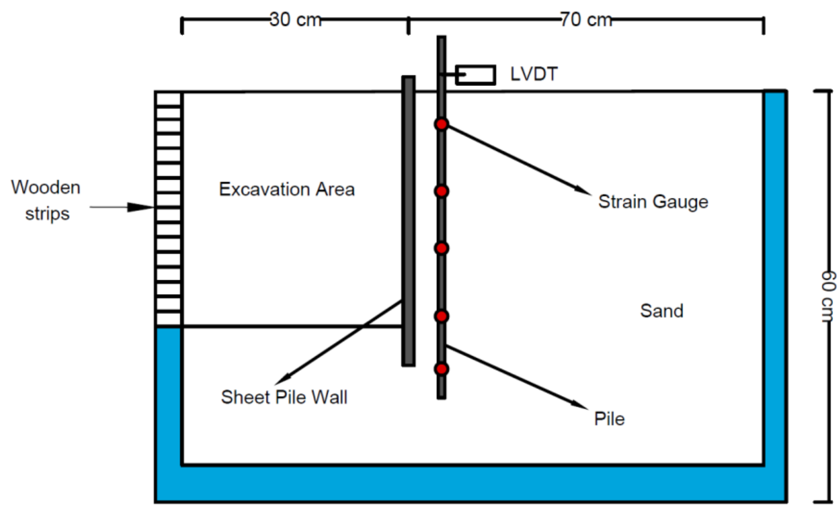

Figure 2.3. Illustrations of model tests performed by Madhumathi and Ilamparuthi (2018) (modified after, Madhumathi and Ilamparuthi, 2018).

Sharafi and Sojoudi (2016), investigated the behavior of sandy slopes subjected to surcharge loads using both experimental and numerical methods. They utilized small-scale physical modeling of slopes made up of loose sand subjected to surcharge loads. They also incorporated digital imaging with particle image velocimetry (PIV) and 3D numerical modeling to investigate slope behavior under surcharge loading. The study examined the effects of various factors on the pile performance. They compared the factor of safety (F_s) and critical failure surface locations of both natural and pile-stabilized slopes. The experiments were conducted in a tank with dimensions of 1.1 m in length, 0.3 m in width, and 0.6 m in height. To attain a uniform and homogeneous D_R, a dry pluviation system was utilized. Digital images were captured from the front side of the testing tank in the testing process. The paper does not explicitly mention how the scale ratio or particle size effect were considered.

El Sawwaf (2005), performed a comparative study to investigate the two (2) methods for stabilizing sandy slopes: using a row of piles or a sheet pile using physical model tests. The presented paper describes laboratory model tests conducted to investigate the behavior of a strip footing supported on a row of piles and a sheet pile-stabilized sandy slope. Several parameters were varied in the study, including pile diameter, pile length, pile spacing, location of the pile row, height of the sheet pile, location of the sheet pile, and location of the footing relative to the slope crest. The laboratory testing was conducted in a test box with dimensions of 1.0 m x 0.50 m in plan view and 0.5 m in height. The sand used in the study was medium to coarse sand, which was washed, dried, and sorted by particle size. Model piles made of steel with different lengths and diameters were employed, while the sheet piles were 3.0 mm thick and made of wood, varying in height. The paper also mentions the effects of scaling. Due to scale effects and the nature of soils, especially granular soils, the behavior observed in laboratory models may not precisely replicate that of the prototype. The main aim of this study was to compare the capacity improvements achieved in each case and determine the most efficient method. Initially, the bearing capacity of the footing on the natural slope cases was determined and compared with that of stabilized slopes. The results were then analyzed to understand the effect of each parameter. The findings indicate that stabilizing the earth slope using a row of piles or a sheet pile significantly improves the bearing capacity of the strip footing. This improvement is more pronounced when the pile spacing decreases and the pile length increases, with further enhancement achieved by increasing the pile diameter. The study demonstrated that both methods improved the stability of the slopes and the bearing capacity of strip footings placed on the slopes. However, the overall improvement achieved by using a sheet pile to stabilize the earth slope was better than using a row of piles. Accordingly, the utilization of a sheet pile was determined as a more effective stabilization technique than the row of pile option.

The study conducted by Rathod et al. (2019), aimed to explore how the behavior of the slope-pile system is influenced by its L_p/d_p ratio and slope angle (β). To incorporate the effects of β and L_p/d_p ratios on maximum bending moment on pile, an empirical equation was developed using multiple regression analysis and provides correction factors for maximum bending moment on pile for various L_p/d_p ratio and β conditions. Basic laboratory tests were conducted on the soil used in the tank, and the soil was classified as CH, which refers to fat clay, per ASTM D2487-06 standard (ASTM, 2006). According to observations of Poulos and Davis (1980), the influence zone of the pile in soft clay typically extends ten times the pile diameter ($10d_p$) beneath the pile tip. Accordingly, to eliminate the boundary effects, the size of the testing tank used for the model tests was chosen as 2 m x 1 m x 1 m, based on the influence zone beyond the pile tip. The laboratory physical model tests were conducted using an aluminum model pipe pile with a length of 810 mm, an outer diameter (d_p) of 25.46 mm, and a wall thickness of 1 mm. The load was applied at the pile head, and deflections were measured using dial gauges. Strains along the pile were also measured by strain gauges with the use of a data logger. To simulate the model pile of a prototype pile, Buckingham's π-theorem was utilized. In the analysis five (5) pile variables were considered: embedment length of pile, L_p, cross-sectional area, modulus of elasticity of pile (E_p), and lateral force. These variables were used to develop a relationship between the model pile and the prototype pile to scale the experimental results appropriately. The results showed that when β changes from level ground to various angles, the lateral load pile capacity changes for different L_p/d_p ratio. However, a ground inclination about 11.30˚ (1V:5H) reduces the lateral load capacity by only about 1.5–2%, indicating minimal impact on lateral load resistance.

Muthukkumaran and Begum (2015) investigated the impact of β on the lateral load capacity of piles and developed p-y curves through laboratory experiments. The response of the prototype structure was analyzed using Buckingham's π-theorem; considering the lateral deflection in the prototype is a function of the scale factor, which is 40 times the lateral deflection of the model pile. The experimental study was conducted in a steel tank with dimensions of 2 m x 1 m x 1 m. An aluminum pipe with an outer diameter of 25.4 mm and a wall thickness of 1 mm was selected as the model pile. Electrical resistance type strain gauges were installed on the model pile, and a load cell was used to measure the applied load. Figure 2.4 provides a simple sketch of the experimental setup. The test tank was filled with sand using a pluviation technique to a depth of approximately 150 mm. Sand was poured in layers, each approximately 200–250 mm thick. Then the lateral loads were applied to the pile head. The procedure was repeated until the pile reached a displacement of 5 mm (equivalent to 20% of the pile diameter) at ground level. Vertical settlement was found to be negligible and Linear Variable Differential Transformer (LVDT) was used to measure the horizontal displacements. Lateral deflection and strain readings were recorded for each applied load increment. The results indicated that irrespective of the soil density and L_p/d_p ratio, the lateral load capacity is significantly reduced when β of the ground surface increases. The soil resistance was found to increase with an increase in D_R of the soil and L_p/d_p ratio of the pile. However, the lateral resistance of the soil depth beyond 24 d_p is not significantly affected by these parameters and p–y curves do not change. Also, it is important to note that this study did not explain the differences in soil structure interaction behavior between the model and the prototype, nor did it consider the effect of mean particle size of soil to pile. These factors may influence the observed results and should be considered in future research.

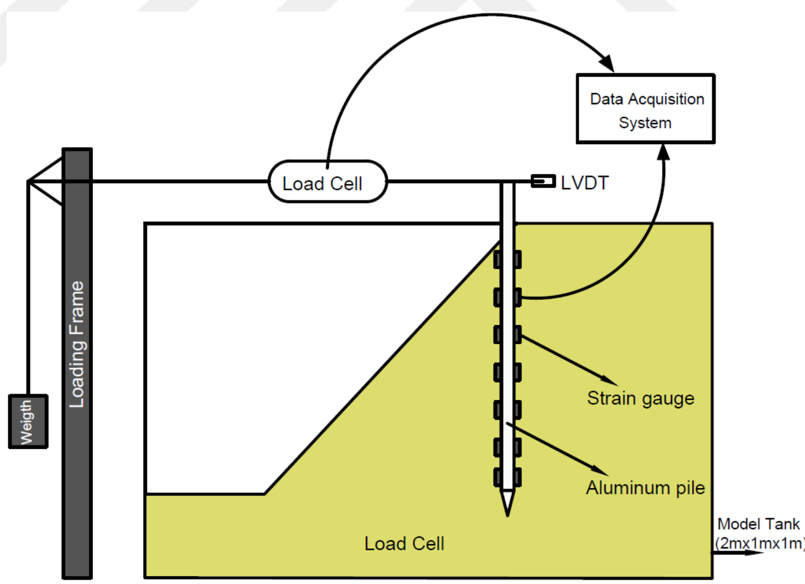

Figure 2.4. Illustration of experimental setup used by Muthukkuamran and Almas Begum, (2015).

Mazaheri et al. (2021) conducted a comparison between numerical analysis and experimental studies. The F_s of the slope model was determined as 1.35~ 1.37 in its initial state. By using image processing technique, new F_s values were recorded as β increased. The main objective of this study was to compare numerical analysis results with the findings from experimental studies by utilizing laboratory equipment and an image processing system. To facilitate the experiments, a container box with dimensions of 1.5 m × 1.5 m × 2 m was manufactured. The box was constructed with 10 mm thick glass on its two (2) sides made of to monitor the behavior of the earth slope during the tests. With these dimensions, earth slopes with heights up to 1.2 m could be modeled at a scale of 1/10. Figure 2.5 illustrates the physical model of the slope stabilized with piles in this study. Following Wood et al. (2002) methodology, the modulus of elasticity of the materials used in the laboratory models of the piles was adjusted to correspond to the stiffness of the piles in the prototype. The entire movement of the slope was recorded using a digital camera placed in front of the slope. Pile-stabilized slopes were tested with various pile distances ranging from one (1) to five (5) times the diameter of the piles, and the displacements were video-recorded as the β increased.

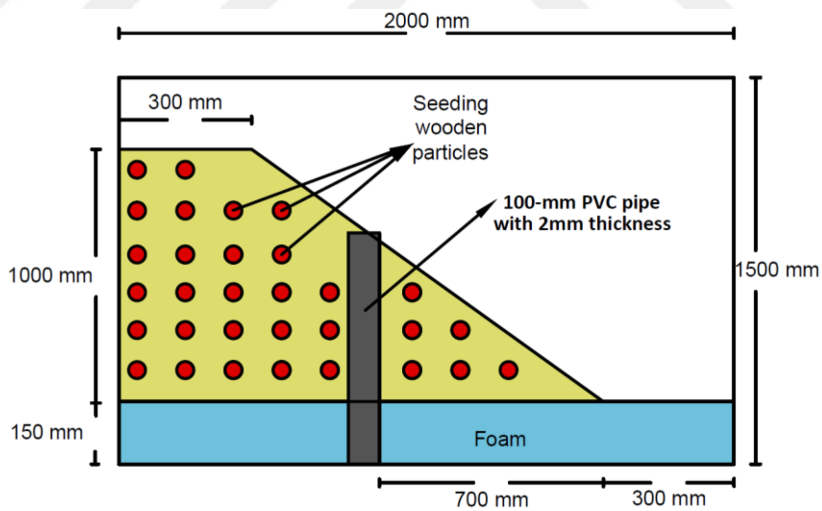

Figure 2.5. Illustration of slope stabilized with pile test by Mazaheri et al.(2021) (modified after Mazaheri et al.,2021).

Khati and Sawant (2021), examined the behavior of pile groups in sandy slopes. The effect of D_R, β, and pile group position on the slope stability was examined. In this study, a total of 23 tests were conducted on sandy soils, considering three (3) different D_R values of sand, three (3) β values, and four (4) positions of the pile group relative to the crest of the slope. The dimensions of the aluminum piles were d_p = 25 mm and L_p = 750 mm. Out of the four (4) piles, two (2) of them were instrumented to measure the bending moment, with six (6) strain gauges placed along the length of the pile at intervals of L_p /8 from the very top of the pile down to $6L_p/8$. Pile head displacements were recorded using LVDTs in contact with the pile cap. The experiments were performed in a tank with dimensions of 2.50 m × 1.22 m × 1.12 m, with one side left open. An illustration of the instrumentation plan and experimental setup is shown in Figure 2.6. In order to minimize the effects of grain size on the results, a fine sand was selected in this study as such, the ratio of pile diameter to mean particle size of sand (d_p /d_{50}) was 90.9. The results showed that pile position on slope has significant effect on pile capacity.

.

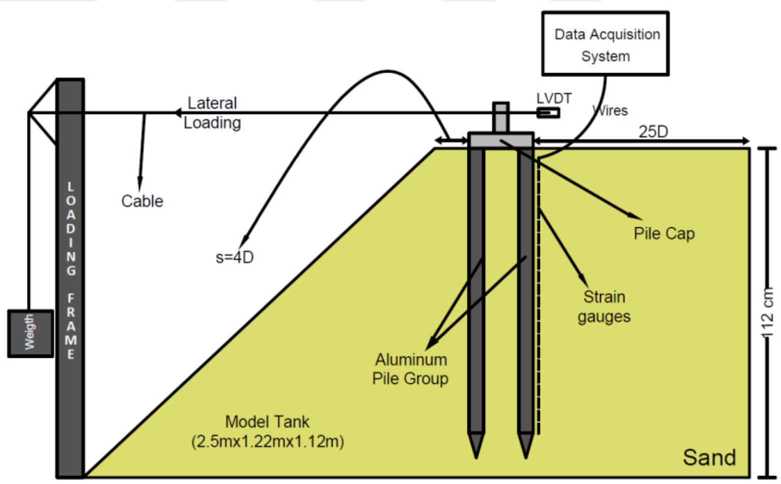

Figure 2.6. Layout of model by Khati and Swanti (2021) (modified after Khati and Sawant, 2021)

Kahyaoglu (2010) performed reduced-scale model tests to understand the behavior of flexible piles embedded in a sliding soil mass. In the tests, a large box filled with soil was designed to slide on an inclined surface with a weak interface. Flexible aluminum pipes were used as piles in the model tests. Piles were embedded in the box and their bottom portions were fixed. A simple sketch in Figure 2.7 shows the experimental setup in this study. The results of this study showed that, each pile behaved like a single pile without arching effects for both cases when the spacing between the piles is greater than eight (8) times the pile diameter.

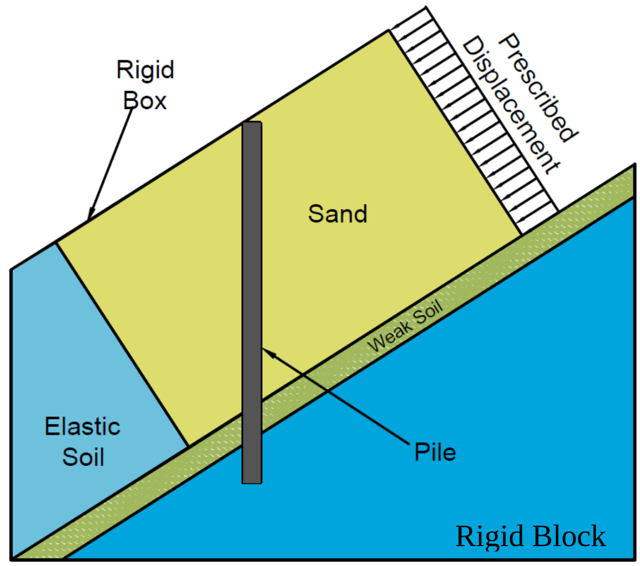

Figure 2.7. Illustration of experimental setup used by Kahyaoglu (2010) (modified after Kahyaoglu, 2010).

He et al. (2020), developed a model simulating a landslide site and investigated the behavior of piles against sliding. To model the conditions of the Majiagau landslide, two (2) consistent setups were constructed in the tests. Each model consisted of six (6) piles, representing a total of 17 piles found in the actual landslide site located in the Three Gorges Reservoir. The landslide-pile model was 2.70 m in length and 1 m in width. The slide zone had an average thickness of 40 mm, while the slide mass had a thickness of 0.32 m. The six (6) piles had a length of 0.57 m and cross-sections measuring 50 mm × 75 mm. Scaling factors of material parameters were derived by the Buckingham π-theorem and dimensional method. To establish consistent ratios of physical parameters, three (3) fundamental parameters: geometry, density, and acceleration of gravity were selected as the basis and were defined as 40, 1, and 1, respectively. The scale factor of modulus of elasticity, cohesion and stress was also 40. Six (6) piles, made up of polyesteramide material with modulus of elasticity of 0.1 GPa, were placed in both tests. A laser scanner and a video camera were utilized to obtain the surface deformation of the landslide-pile model in two (2) of the tests, and pore water pressure gauges were buried face up in the slide zone at different elevations.

Fu et al. (2019) investigated the lateral load response behavior of piled bridge foundations and stabilizing piles on steep slopes through a combination of reduced-scale experimental studies and numerical simulations. The scale factor was selected as 40 and Buckingham π-theorem was used. Gravel soil and bedrock were chosen as representatives of the in-situ conditions, with their properties selected to match the actual conditions. The piled bridge foundation and stabilizing piles were made from the steel bar and micro concrete. Model tank size was determined as 2.85 m × 0.9 m × 2.5 m. Strain gauges, soil pressure cells, horizontal displacement gauges are used as measurements devices. Figure 2.8 provides an illustration of experimental setup and instrumentation plan. For the loading program, 5.9 kN was applied to the slope firstly, as horizontal displacement changing ratio was smaller than 0.01 mm/min. The study found that the bending moments in the bridge piles were much lower than those in the back stabilizing piles. This difference was mainly due to the significantly smaller soil movement around the bridge piles compared to the back stabilizing piles. Additionally, the bridge cap restricts rotation, increasing the overall stiffness of the piled bridge foundation.

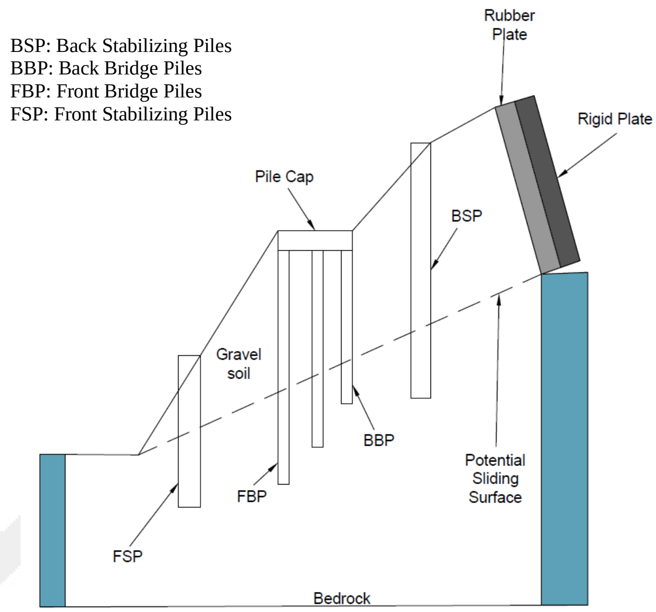

Figure 2.8. Illustration of experimental configuration used by Fu et al., (2019) (modified after Fu et al., 2019)

Lastly, Abdelhalim et al. (2020), examined the behavior of piles located adjacent to sandy slopes contaminated with oil. The main factors investigated include the thickness of the contaminated sand layer, the amount of oil in the soil, and the size of the piles, in essence, pile length to pile diameter (L_p/d_p). The experimental tests were conducted in a tank made of mild steel. The tank had inner dimensions of 1000 mm in length, 500 mm in width, and 600 mm in height. These dimensions were chosen to ensure that the expected failure wedges around the tested pile do not reach the tank walls. Marks were placed at 50 mm intervals on the inside walls of the tank to help with the setup and configuration of the sandy soil layers. The vertical borders of the tank were supported using roll-formed steel angles at the top and bottom. Figure 2.9 provides a visual representation of the experimental setup. To minimize friction between the tank walls and the soil, the inner walls of the tank were smoothed. The model piles used in the experiment were made of roll-formed steel pipes with an outer diameter of 21 mm and an inner diameter of 17.4 mm. These pipe piles placed in the soil had lengths of 350 mm and 450 mm. The L_p/d_p ratio was 16.6 for the shorter piles, simulating rigid short piles, and 21.4 for the intermediate piles. A lateral load of 5 N was applied to the pile. The load was transferred through a high-tension steel wire with a diameter of 2 mm, which was attached to the pile head using an eye bolt. Two (2) high sensitivity dial gauges, with 0.01 mm accuracy, were used to measure the horizontal deflections of the piles. The objective was to validate the consistency of experiment results using FE analysis. The findings demonstrated a strong agreement between the FE results and the experimental test results, confirming the reliability and suitability of the FE analysis. Model tank dimensions, pile properties, soil types, the measurement techniques and instruments implemented in prior studies are systematically summarized in Table 2.2.

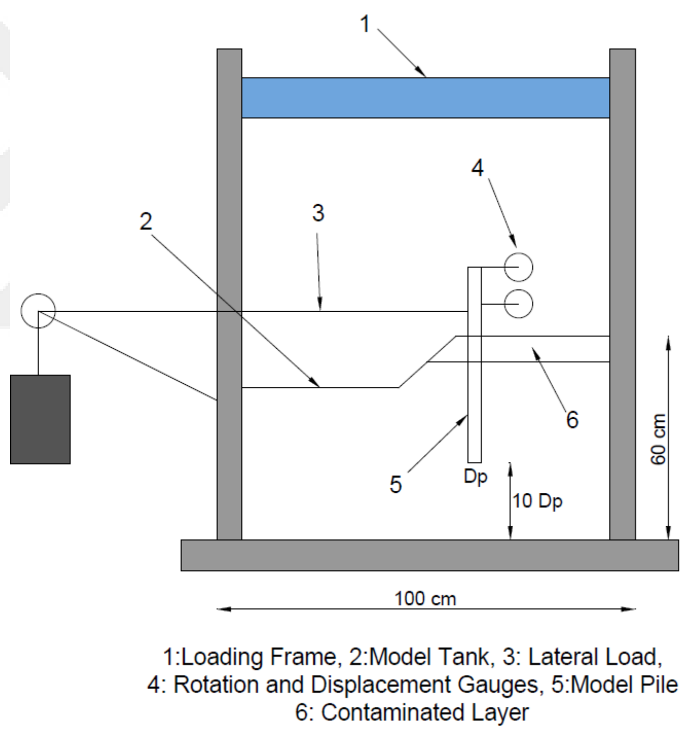

Figure 2.9. Illustration of the model by Abdelhaim et al. (2020) (modified after Abdelhalim et al.,2020)

Table 2.2. Summary of model tests that investigate the behavior of slopes stabilized with piles

No	Study	Model Tank Dimension (LxWxH)	Soil Material	Scale Method and Geometric Factor	Pile Material and Dimensions	Measurement Devices
1	Abdelhalim et al. (2020)	1 m x 0.5m x 0.6m	Sandy soil	Not specified	Steel Pile, Outer diameter 21 mm, Inner diameter 17.4 mm	High sensitivity dial gauges
2	Fu et al. (2019)	2.85m × 0.9m × 2.5m	Gravel soil and bedrock	1/40	Steel bar, microconcrete	Strain gauges, soil pressure cells, horizontal displacement gauges
3	He et al. (2020)	2.70m x 1m x 1.28m	-	Buckingham's π-theorem 1/40	Polyesteramide material, 50 mm × 75 mm	Laser scanning, video cameras, pressure gauges
4	Kahyaoglu (2010)	2m x 1.2m x 0.5 m	Sand	Buckingham's π-theorem 1/20	Aluminum pipes, Outer diameter 20 mm, Thickness 1.4 mm	Displacement transducers, strain gauges, load cells
5	Khati and Sawant (2021)	2.50 m × 1.22 m × 1.12 m	Sandy soil	Not specified	Aluminum piles; Diameter 25 mm	Strain gauges, LVDTs
6	Mazaheri et al. (2021)	1.5 m × 1.5 m × 2 m	Sand	Wood, Scale of 1/10	PVC piles, 10mm diameter,	Digital cameras
7	Muthukkumaran and Begum (2015)	2 m x 1 m x 1 m	Sand	Buckingham's π-theorem 1/40	Aluminum pipe, Outer diameter 25.4 mm, Wall thickness 1 mm	Strain gauges, LVDTs

Table 2.3. Summary of model tests that investigate the behavior of slopes stabilized with piles (cont.).

8	Rao and Nasr (2010)	0.8m x 0.3m x 0.6m	Sand	Not specified	High tensile steel bars, Diameter 6 mm	Dial gauges
9	Raja and Muthukkumaran, 2021	2m x 1m x 1m	Loose sand	Not specified	Aluminum pile Outer diameter 25.4 mm inner diameter 19.4 mm	Electrical resistance foil-type strain gauges, LVDT
10	Rathod et al., 2019	2m x 1m x 1m	Clay	Buckingham's π-theorem, 1/25	Aluminum pile Outer diameter 25.4 mm 1mm wall thickness	Dial gauges
11	El Sawwaf, 2005	1m x 0.5m x 0.5m	Medium to coarse sand	Not specified	3mm sheet pile	-
12	Sharafi and Sojoudi, 2016	1.1m x 0.3m x 0.6m	Loose sand	Not specified	-	Digital imaging, PIV, 3D modeling
13	Madhumathi and Ilamparuthi, 2018	1m x 0.6m x 0.6m	Medium dense sand	Wood, 1/20	Aluminum pile 19.05 mm diameter	Strain gauges, LVDTs
14	Ozkahriman and Wartman, 2007	1.68m x 1.18m -	Clay	Iai, 1/22	Not used	Displacement potentiometers, accelerometers

2.5. Measurement Techniques in Physical Model Tests

To measure displacements and deformations accurately in the experiments, various instruments and measurement techniques were utilized in previous studies, which are summarized in Table 2.2. Generally, LVDTs were employed to measure the pile head displacements. Strain gauges were attached along the piles to assess the deformations and to calculate the stress distribution along them. Accelerometers were strategically placed on soil to record ground motion. Additionally, load cells were integrated with the loading plates to measure the applied loads. Furthermore, PIV was used as an advanced optical method to observe and analyze the deformation patterns in the soil. Photographs were taken continuously during the tests, enabling a detailed examination of the displacement field and particle movements in PIV analysis. PIV analysis in geotechnical engineering is generally performed using MATLAB-based software such as geoPIV (White et al., 2003) and geoPIV RG (Stanier et al., 2016). The analysis process begins by defining an Area of Interest (AOI) that encompasses the region of deformations, which is then subdivided into a grid of square patches. The size of these patches is a crucial choice for the user, as it impacts computation time and its detailed resolution. Smaller patches offer more detail but may hinder recognition of differences, while larger patches reduce computation time but might lead to less detailed analysis.

Several research studies used PIV analysis in slope stability analysis, exemplifying its use in understanding deformation and strain behavior in various applications. Stanier et al. (2016), studied a 30 mm diameter flat footing, representing a prototype that has a 6 m diameter, and was subjected to punch-through tests on a 20 mm deep sand layer overlying clay using a 200g centrifuge test. The experiment involved capturing 550 images at a frequency of 5 Hz, with artificial texture applied to the model's exposed face using the optimal artificial seeding ratio (ASR) concept from Stanier et al. (2016). Several specific recommendations were given for ASR, such as seeding particles should have a sufficient diameter within the images captured for each experimental setup (*i.e.* d_{50} /pixel size >4). Generally, the exposed surface of geotechnical models are seeded with dyed sand that has an ASR value between 0.3 and 0.7. This range helps to ensure that seeding particles are distinguished from one another while photographing.

3. DEVELOPMENT OF EXPERIMENTAL SETUP AND RESULTS OF CALIBRATION STUDIES

This study focuses on the development of a small-scale physical model and the model tests performed to understand the behavior of loaded sandy slopes and loaded sandy slopes stabilized with piles. In physical model tests, scaling and selection of model components are important aspects. Accordingly, the initial part of this research study focused on developing the small-scale test model setup. This Chapter initially explains the development of the experimental setup including the definition of the prototype, the scaling factors used, the selection of the test box, and the model piles. Later, the engineering properties of the fill sand were discussed based on the results of the laboratory tests. Lastly, the pluviation technique was used for placing the sand layers in the model tank. To achieve the target density of sand in model tests, a small calibration box was designed and manufactured from wood. The initial density calibrations for the pluviation method was performed in this wooden box. The results of this calibration process were summarized in this Chapter. The Chapter concludes with a presentation of the developed overall test setup, including the measurement and data acquisition systems.

3.1. Prototype and Small-Scale Physical Model Details

A prototype was designed to mimic an assumed field scenario. The prototype consisted of an 8-meter-high sand with a slope angle (β) = 30˚. Local loads were considered in the design to simulate surface loading effects. A rigid load plate of 5 m by 10 m was planned to attain the local loads. Additionally, to improve the stability of the slope, pile stabilization was considered in the design. 1.5 m-diameter drilled shafts that are made from C30 concrete were considered. These piles were strategically placed at the upper-middle part of the slope to maximize stability and workability, based on the results of the numerical analysis presented by Tekdemir (2023) and Mamedov (2024). To determine the total pile length, the position of the pile head and the required socket length were considered carefully. Considering that ~ 40% of the pile length was socketed into a dense sand layer to provide sufficient anchorage and stability, a pile length of 20 m was selected.

To facilitate detailed observations and measurements in the course of this research, these full-scale prototype conditions were replicated in a small-scale physical model. The model's scale and the materials used were carefully selected to accurately represent the behavior of the full-scale prototype under similar conditions. As summarized in the literature review, various scaling techniques corresponding to various scaling factors were used in similar studies. To ensure ease of application and practical feasibility, a 1/40 scale factor was selected for this study, consistent with the methodology compiled by Wood et al. (2002). All the design parameters for the prototype and the developed small-scale physical model are provided in Table 3.1.

Table 3.1. Summary of prototype and physical model dimensions.

Design Parameters	**Symbols**	**Prototype (m)**	**Model (cm)**
Pile diameter	d_p	1.5	3.7
Pile socket length	L_s	8	20
Pile length	L_p	20	50
Toe length	T_l	19.4	48.5
Layer thickness below toe	T_h	20	50
Foundation width	b	5	12.5
Foundation length	l	10	25
Distance between slope crest and foundation	d	0	0
Slope height	H	8	20
Slope angle	β	30˚	30˚
Ratio of socketed pile length to pile length (%)	%s	40%	40%

3.2. Small- Scale Physical Model Test Tank

The experiments were conducted using a custom-designed model tank with dimensions of 1.2 m (length) x 0.9 m (width) x 0.8 m (height) to minimize the boundary effects. Figure 3.1 provides a photo of the model tank and its dimensions. The model tank features an open top for easy access for soil placement. A central steel beam spans across the top of the box, allowing it to be carried conveniently. The base and frame of the box were constructed from durable steel to ensure stability and rigidity.

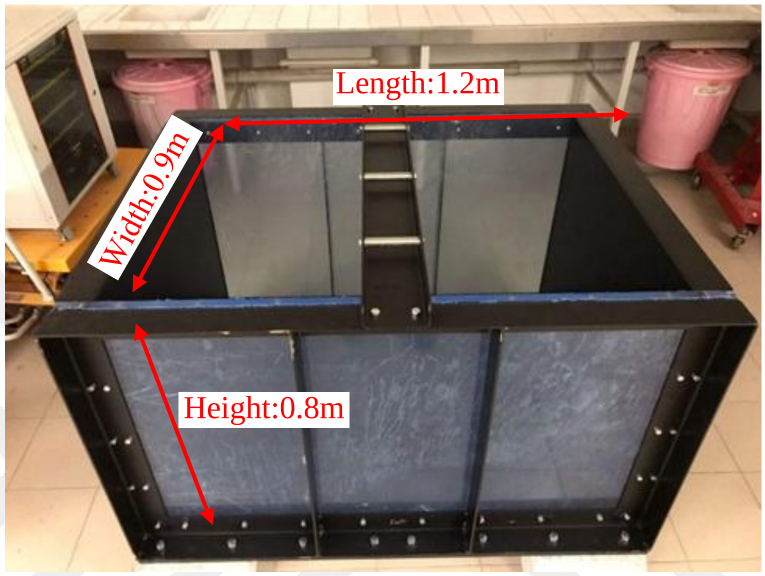

Figure 3.1. Photos of the model tank.

To prevent any movement of the side surfaces during the experiments, two (2) additional steel columns were incorporated into the design. The front and rear surfaces of the tank were fabricated from 10 mm-thick Plexiglas, providing clear visibility while maintaining structural integrity. To protect these Plexiglas surfaces from potential damage during testing, 2 mm acetate sheets were adhered to the Plexiglas using Vaseline to the corners and sides of the acetate. Afterwards, to prevent sand to intrude between acetate and plexiglass, sides of the tank were sealed with tape.

3.3. Purpose and Design of the Slope Model Mold

A mold was designed and manufactured to create the slope surface required for small-scale physical model tests. The design process was iterative, progressively refined until the final mold configuration met all the requirements, including allowing the pile placement in the model. The designed mold consists of five (5) wooden segments, each with dimensions of 10 cm by 88 cm by 1.8 cm. The mold length was selected as 88 cm to ensure that it fits comfortably within the model tank, which has a width of 90 cm. This slight reduction allowed for a working space to facilitate the placement and adjustment of the mold. The mold was structured in multiple segments for several reasons. Firstly, segments allow the adjustment of the surface height as needed. These segments also ensure a relatively smooth slope surface generation. Furthermore, this design enables even the filling of sand within the tank. By using this mold, the sand could be spread to all areas of the tank without obstruction. Also, each segment was drilled at predetermined locations to allow steel rebars to pass through them, ensuring alignment and structural integrity. Two (2) rebars bent to a 30˚ angle, were prepared to secure the structural integrity. Figure 3.2 shows the rebars and a wooden segment, before the construction of the slope surface.

The assembly process began by threading the first two (2) wooden segments onto the rebars. These segments remain stable during the experiment. The remaining segments were then carefully positioned in sequence. Each segment was then adjusted to achieve the desired height and sand level for the test. This step-by-step process ensured that the stability of the mold was maintained, and the flexibility needed for precise slope configurations could be attained. Figure 3.3 shows the completion of sand placement before the placement of the mold.

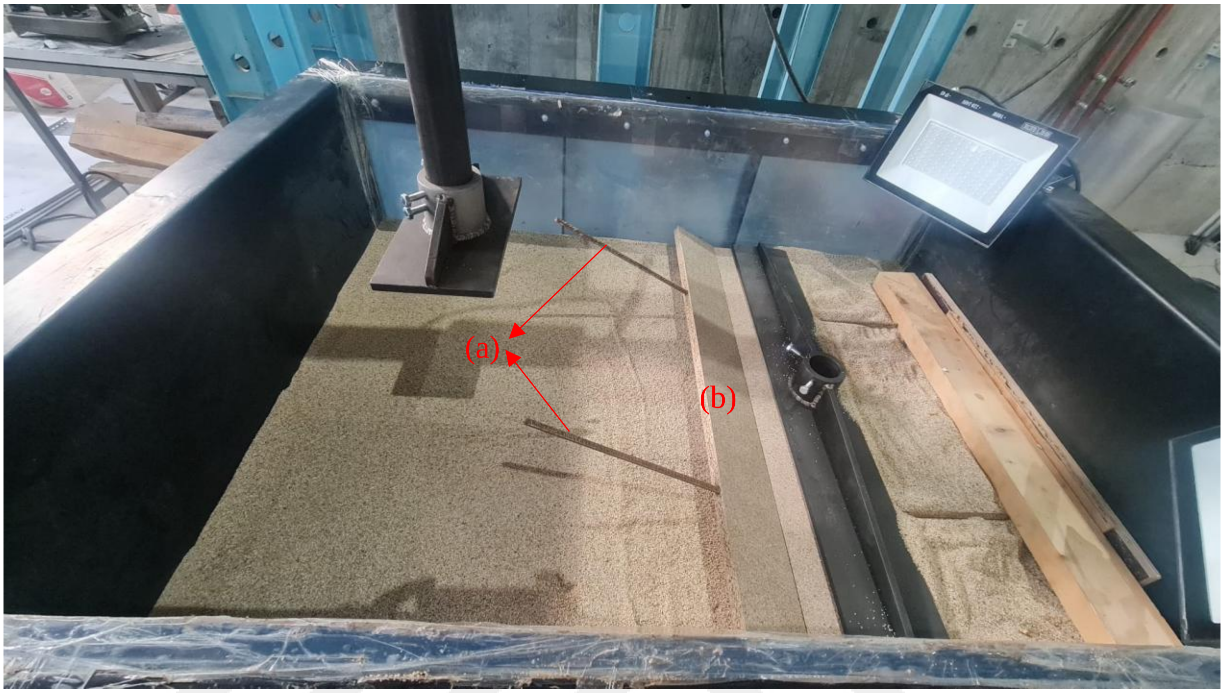

Figure 3.2. Picture depicting the mold parts: (a) rebars, (b) wooden segments.

Figure 3.3. Picture depicting assembled mold after soil placement.

3.4. Loading Plates

The loading plates used in this study are crucial components of the test apparatus, designed to ensure uniform load distribution on top of the sand. The plates were constructed from stainless steel, selected for its high strength and resistance to deformation under loads. This material choice guarantees that the plates maintain their integrity in loading while also ensuring loads are applied uniformly on the sand layer. Each loading plate had a socket hole on its top surface that allowed its connection to the rod of the loading system.

Two (2) different loading plates were manufactured as a part of this project: *(i)* one for plane-strain conditions and *(ii)* one for local loads. The plane-strain loading plate, which simulates plane loading conditions had a length almost identical to the width of the model tank. The length was only reduced by a few centimeters to prevent interference with the tank's plexiglass sides. The second loading plate was used to simulate local loading conditions with limited dimensions. Both loading plates were integral to the experimental setup, with dimensions carefully tailored to suit test conditions accurately. The photographs of the plane-strain and the local loading plates are shown in Figure 3.4a and Figure 3.4b, respectively. Please note that even though both plates were constructed for the project, only the local loading plate was utilized in the experiments presented in the content of this thesis.

(a)

(b)

Figure 3.4. Loading plates: (a) plane-strain loading plate - 12.5 cm x 88 cm, (b) local loading plate - 12,5 cm x 25 cm.

3.5. Pile Properties

To create a model of the pile that accurately represents the full-scale prototype, it was important to follow scaling methods, especially for slender elements, such as the piles in the model. The prototype pile was considered to include 1.5 m – diameter drilled shafts manufactured from C30 concrete. For the model, a scaling factor of 1/40 was utilized, which means the relevant properties of the model pile should be reduced by a factor of 40.

Since the piles resist both horizontal and vertical loads, it is required to scale a parameter that is a measure of its stiffness. Accordingly, the pile's flexural rigidity, that can be calculated by multiplying the elastic modulus of pile (E_p) and moment of inertia of the pile (I_p) was investigated. Initially, $E_p \times I_p$ of the full-size concrete pile was calculated. Then, scaling methods presented by Wood et al. (2002) were used to find the appropriate scaling factor for this study. By dividing the prototype's $E_p \times I_p$ into this scaling factor, the $E_p \times I_p$ needed for the model pile was estimated as 26 GPa×cm^4. This flexural stiffness value was targeted for the piles used in the model. For this purpose, various pile designs and materials were explored to match this required flexural rigidity. Table 3.2. provides the various options considered for the pile models.

One of the main criteria for the pile model selection was the ease of manufacturing. It is not possible to produce lead and/or aluminum hollow piles in the desired thicknesses. Accordingly, a PVC pipe was selected as the model pile since the material was easy to work with among those considered and closely matched the flexural rigidity needed for the model pile.

Table 3.2. Pile materials and sections considered for the model pile.

	Prototype	Model (1)	Model (2)	Model (3)	Model (4)	Model (5)
Pile Material	Concrete	Steel (Hollow)	Wood (Bar)	Aluminum (Hollow)	PVC Pipe	Lead (Hollow)
E_p (GPa)	35	200	7	70	4	16
Pile Diameter(cm)	150	3.7	3.7	3.7	3.7	3.7
Pile Thickness(cm)	-	3	-	0.1	0.5	0.2
$E_p \times I_p$ (GPa×cm^4)	869,767,107	1565	64	128	26	54

Note: Scale factors for length, density and flexure rigidity of pile are 40, 1 and 33,859,611 as respectively.

3.6. Selection of Sand for the Slope Fill

The selection of the sand for the experiments was guided by three (3) primary factors that affect the processing of the images: particle size, image resolution and color contrast. The first criterion is particle size of the soil. Keeping the soil particle size below some threshold helps ensure that the pile’s interaction with the soil is not distorted by the effects of having overly large individual particles. Abdelhalim et al. (2020) recommended that the ratio of pile diameter to mean diameter of soil should be greater than 30. The purpose of this requirement is to ensure that the sand particles are much smaller than the pile. To avoid scale error between the sand particles and the piles used, the maximum allowable mean diameter (d50) is 1.06 mm, for a pile, dp of 37 mm. Selection of sand has smaller this d50 ensures that the soil particles are sufficiently small relative to the pile, minimizing any discrete effects that could lead to inaccurate modeling of the soil's continuum behavior. Another criterion is image resolution to be able to apply PIV method. For the particles to be clearly visible in photographs, the ratio of

d_{50} to pixel size needs to be greater than 4. Given that a 24 MP camera capturing the entire 80 cm x 120 cm surface results in a pixel size of about 0.16 mm, the mean diameter (d_{50}) of the sand has to be at least 0.64 mm to ensure clarity in the images (Stanier et al., 2016). Finally, the color contrast of the sand particles must be carefully selected to ensure sufficient differentiation from each other in photographs, enabling accurate analysis. Therefore, natural yellow sand was chosen for its visibility and contrast in images (Stanier et al., 2016).

Washed, sieved, and dried sand satisfying all the criteria listed above was acquired for the experiments. To identify the engineering parameters of the selected sand, a series of index tests: specific gravity, gradation, minimum density and maximum density tests were. These tests provided the essential data required for soil classification and density calibrations. Additionally, the shear strength of any soil is critical to evaluate slope stability. Accordingly, shear strength parameters of the sand were determined through direct shear tests and the simplified method proposed by Santamarina and Cho (2001) to determine the critical state of sand.

3.7. Gradation of Sand

To determine the grain size distribution of the sand sample, sieve analysis was conducted following ASTM D6913/D6913M – 17. The test begins with drying the soil sample at 110°C to a constant weight. The prepared sample is then placed on a stack of sieves arranged in a descending mesh size and subjected to mechanical agitation for a specified duration. Figure 3.5 shows the stack of mesh and the mesh's opening sizes used in the experiment. After shaking, the soil retained on each sieve is weighed, allowing the calculation of cumulative percentages (by weight) passing each sieve size. This analysis results provided the opening sizes: d_{10}, d_{30}, d_{50}, and d_{60}, which represent the diameters through which 10%, 30%, 50%, and 60% (by weight) of the sample passes through respectively. The uniformity coefficient (C_u) and the coefficient of curvature (C_c) are also derived from these parameters.

.

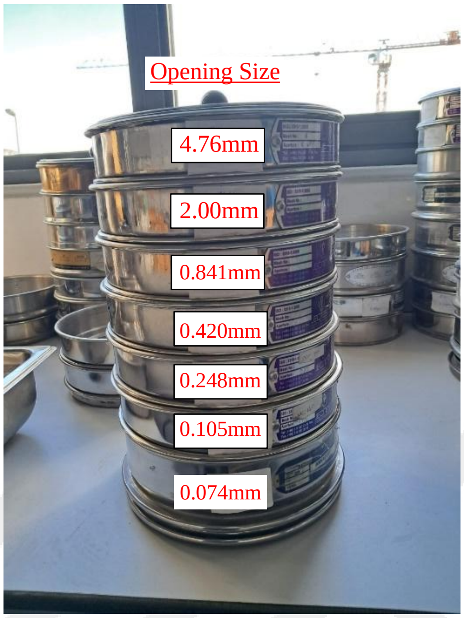

Figure 3.5. Stack of mesh sizes used in sieve analysis.

In this study three (3) air dried sand samples (*i.e.*, sample 1, 2 and 3) and one (1) washed sand sample (*i.e.*, Sample 4) were sieved. The particle diameter (log scale) versus weight percentage % finer graph obtained from the sieve analysis of these four (4) samples are illustrated in Figure 3.6. The grain size distributions were consistent. From these results, mean particle size, d_{50} of the selected sand is calculated as 0.89 mm.

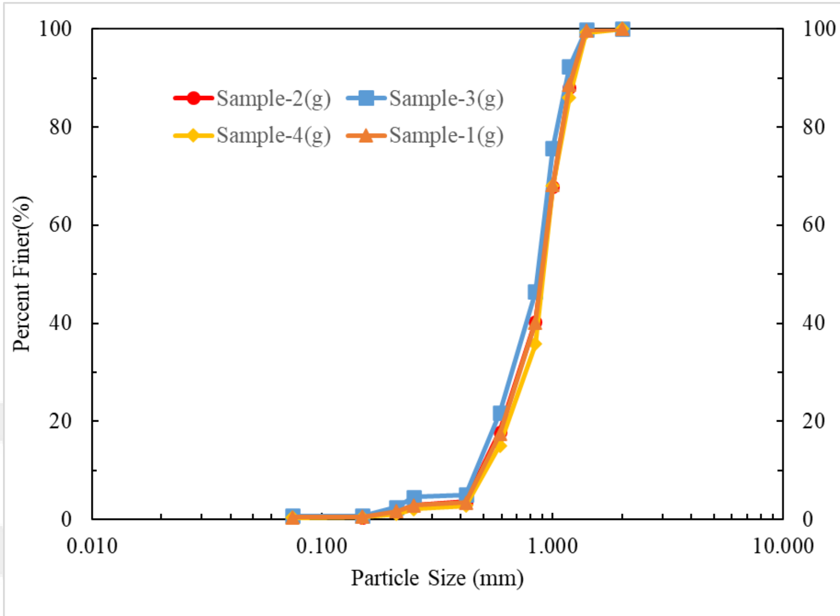

Figure 3.6. Grain-size distribution of sand samples.

3.8. Specific Gravity of Sand

To determine the specific gravity of the sand sample, a specific gravity test was conducted using a pycnometer following ASTM D2320 − 98. The procedure involves weighing a dry soil sample and placing it into a pycnometer partially filled with distilled water. After removing air bubbles using vacuum or boiling techniques, sufficient time was allowed to observe the settlement of the particles and the clear water in the pycnometer. Then the pycnometer is carefully filled with water and sealed. After temperature equilibrium, the pycnometer is weighed. Figure 3.7 shows a picture of the weighed sand samples with distilled water. The test also requires determining the weight of the pycnometer when filled with water only, as well as its empty weight. Using these values, the specific gravity (G_s) of the soil is calculated.

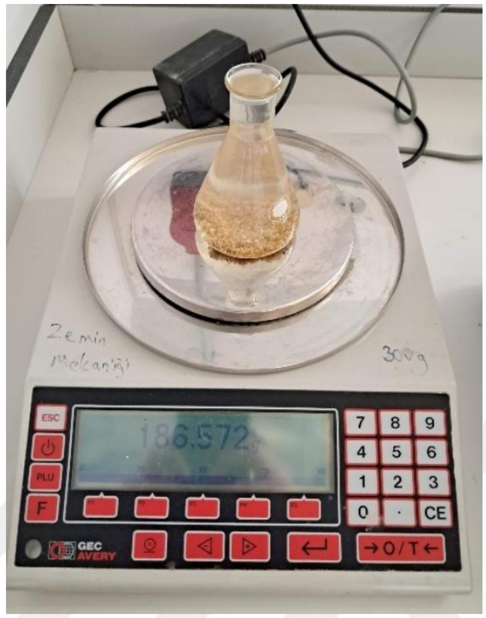

Figure 3.7. The pycnometer filled with both sand and distilled water.

The specific gravity (G_s) values obtained are essential for subsequent calculations of void ratio (e). The specific gravity of the silica sand is calculated as 2.65.

3.9. Minimum and Maximum Void Ratio of Sand

To adjust the D_R of the sand in the model tank, both minimum void ratio (e_{min}) and maximum void ratio (e_{max}) values are required. The values of e_{max} and e_{min} were determined in accordance with ASTM D4253-16e1 and ASTM D4254-16, respectively. The minimum index density is determined by loosely placing the soil into the mold without any densification procedure to achieve the loosest possible state of the test sand. Conversely, the maximum index density is obtained by compacting dry soil into a mold using vibrations under ASTM-specified standard conditions, ensuring the densest possible state. Figure 3.8 shows the mold filled with sand sample, together with the vibratory table.

The densities obtained from these tests are used in D_R calculations. These tests provide critical data points that are essential for understanding the void ratio and the densification of the sand sample under various conditions. Table 3.3. presents the results of the e_{min} and e_{max} tests for the tested sand sample together with the other soil index parameters.

(a) (b)

Figure 3.8. Minimum and maximum density tests: (a) the mold filled with sand weighed for loosest packing, (b) the mold on the shaking table to attain the densest packing of sand particles.

Table 3.3. Index properties of the sand used in slope model.

USCS Classification	Poorly graded sands (SP)
Median Particle Size (d_{50}) (mm)	0.89
Coefficient of Uniformity (C_u)	1.83
Coefficient of Curvature (C_c)	1.17
Specific Gravity (G_s)	2.65
Maximum Void Ratio (e_{max})	0.85
Minimum Void Ratio (e_{min})	0.57

3.10. Strength Parameters of Sand

To determine the peak and end-of-test frictional angle of sand, direct shear test was conducted in accordance with ASTM D3080/D3080M-23. A remolded soil sample, prepared at D_R= 84%, is placed in a shear box, and sheared at normal stresses approximately equal to 100 kPa, 200 kPa and 300 kPa. The sample is sheared with a controlled displacement rate of 0.2 mm/min, until failure occurs. The shear force and displacement measurements are recorded throughout the test. Figure 3.9 shows the horizontal displacement versus shear stress plots for tests performed at the three (3) different normal stresses selected.

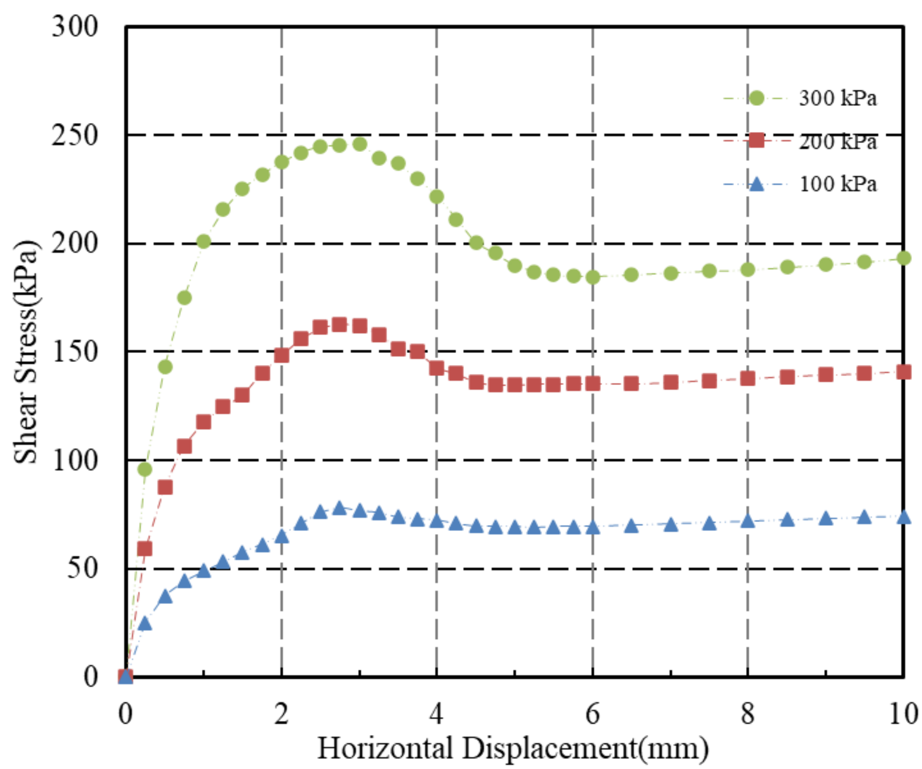

Figure 3.9. Horizontal displacement versus shear stress plots from direct shear tests.

Figure 3.10 (a) and (b) show an end-of-test (ultimate) friction angle of (ϕ_e) and peak friction angle (ϕ_{peak}) envelopes for the soil sample prepared at D_R = 84%, respectively. The strains attained at the end of direct shear tests may not be sufficient to reach the critical state.

Other experimental methods should be employed to accurately estimate the critical state friction angle(ϕ_c). Accordingly, the ultimate states were cautiously reported as end-of-test friction angles herein. The test yielded for the sand sample as ϕ_{peak} = 38.4˚ and ϕ_e=29.6˚.

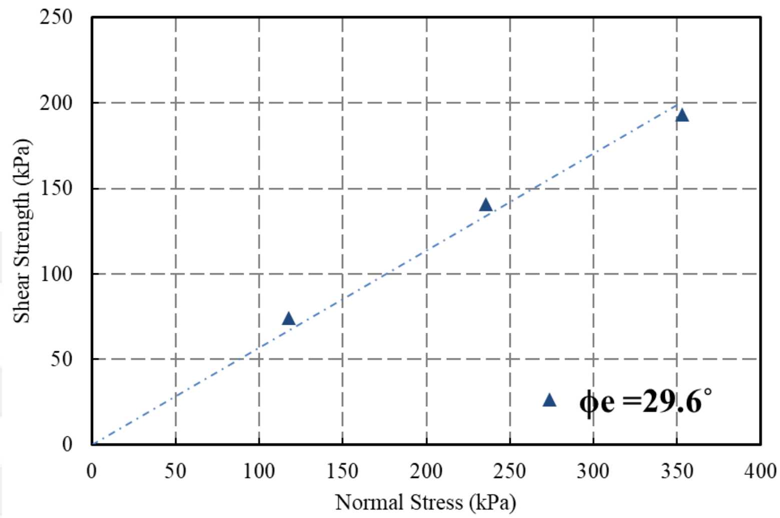

(a)

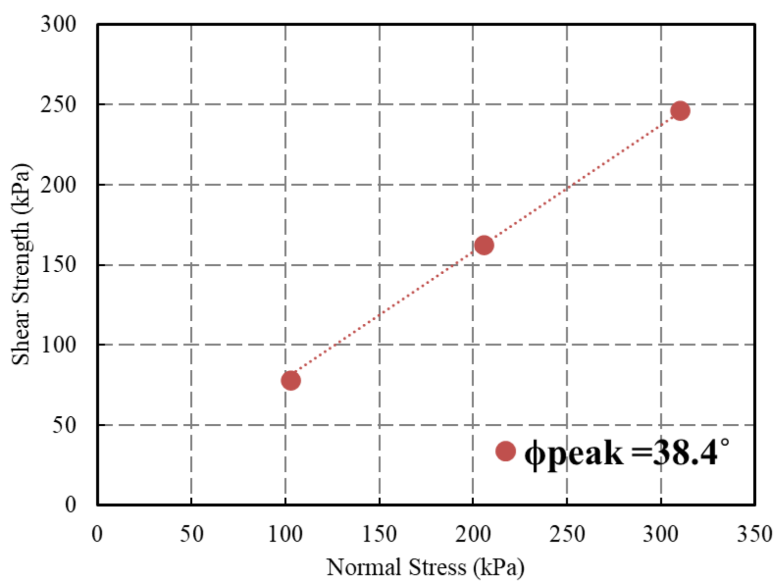

(b)

Figure 3.10. Direct shear test results for the soil sample prepared at D_R = 84%: (a) ϕ_e envelope, (b) ϕ_{peak} envelope.

A simplified method provided by Santamarina and Cho (2001) was also used to determine the critical state friction angle (ϕ_c) of sand. A 1000-mL cylinder is filled with soil and water. The cylinder is then tilted beyond 60° to allow the soil to shift and form a natural slope inside. After reaching the desired tilt, the cylinder is gradually returned to its upright position. After stabilization of the sand surface, the angle is measured at the midpoint of the slope. Figure 3.11 shows the picture taken at the end of this simple procedure. The test is repeated three (3) times, and the average value of critical state friction angle is determined as $\phi_c = 29.5^{\circ}$. This value is very similar to the end-of-test friction angle (ϕ_e=29.6°) from the direct shear test results, indicating critical states were attained at the end test.

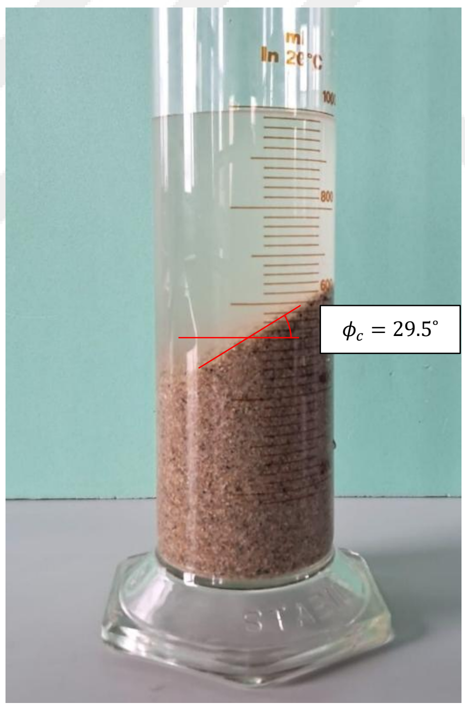

Figure 3.11. $\phi_c = 29.5^{\circ}$ of the sand using the simple test technique proposed by Santamarina and Cho (2001).

3.11. Results of Density Calibration Tests for Sand Pluviation Technique

In model tests, it is important to achieve the correct target densities in the model tank. Achieving the correct and uniform sand density in model tank, ensures the load is properly transferred to the lower sand layers and eliminates erroneous results. To achieve consistent D_R values, the sand was placed using the pluviation technique. This method involves allowing the sand to fall from a controlled height through a device with specific opening sizes. The density of the sand varies based on the critical parameters of this method: pluviation height, opening size and deposition speed.

The pluviation height is defined as the vertical distance through which sand particles fall before deposition. Studies have shown that increasing the pluviation height up to a certain threshold increases the D_R due to the higher impact velocity of particles upon deposition. For instance, experiments demonstrated that increasing the drop height from 0.1 to 1.0 meters results in a linear increase in D_R (Abdollahi, M. and Bolouri Bazaz, 2017). The opening size of the pluviation device, referring to the dimensions of the apertures through which sand particles pass, directly influences the mass of sand deposited per unit area. Larger openings allow a higher flow rate, leading to lower D_R due to increased deposition intensity. Conversely, smaller openings reduce the particle flow rate and form denser specimens. For example, utilizing rain nozzles with different opening sizes has been shown to produce varying D_R in sand specimens, with smaller openings generally yielding higher densities (Li and Zhang, 2022). Deposition speed, or the rate at which the pluviation device moves horizontally during sand deposition, also affects the uniformity and density of the specimen. Slower deposition speeds facilitate the controlled placement of sand particles, resulting in higher D_R and uniform layers. In contrast, higher speeds may lead to non-uniform deposition and lower densities (Wu et al., 2022).

One of the primary objectives of the calibration of the equipment and the sand pluviation technique is to ensure that the correct critical parameters (*e.g.*, drop height, opening) are attained in the equipment. This is required to help maintain uniform sand layers with consistent target D_R are achieved in the model tank. To accomplish this, the calibration procedure was executed to obtain the desired D_R. A wooden box with 9.83 cm × 36.2 cm × 36.2 cm was utilized for calibration purposes. Two (2) different tanks which contain sand were employed as sand containers: a PVC tank and a metal tank both combined with plastic pipes approximately 1 meter in length. Figure 3.11 illustrates the setup for the calibration technique using the metal tank.

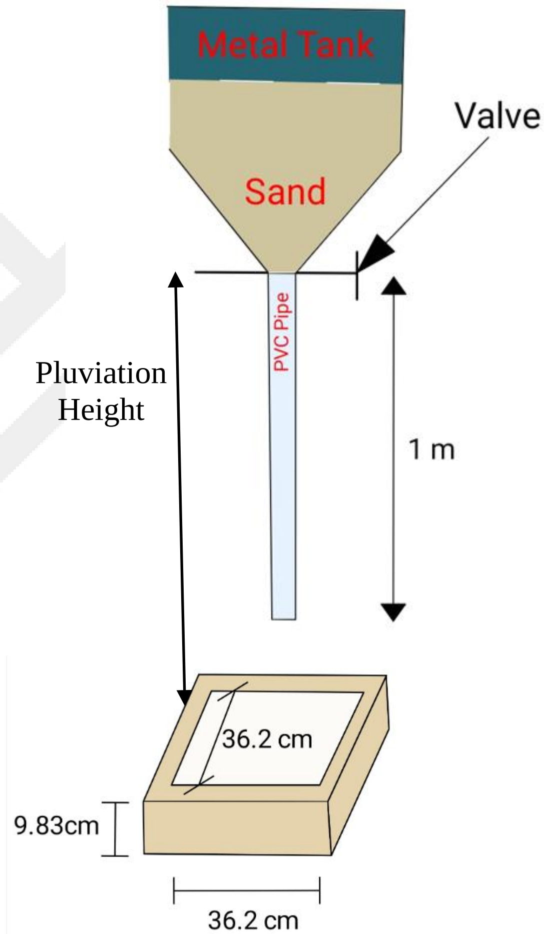

Figure 3.12. Illustration of the pluviation apparatus and the setup used for calibration tests.

The calibration process involved a pluviation apparatus, where sand was discharged through the plastic pipes connected to the polycarbonate (PC) and metal tanks. The plastic pipe was appropriately selected appropriately to control the movement of the pipe. The pluviation height was adjusted with the help of the crane. A valve was installed at the junction of the pipe and tank, allowing for manual control over the amount of falling sand. Either by fully or partially opening the valve, sand raining process was precisely adjusted. While pouring sand into the wooden box, the pipe was maintained in a vertical position to simulate free fall. Figure 3.12 shows the sand placement process in the wooden box during calibration tests. Additional care was employed to keep a consistent pace while moving the pipe across the top of the box to ensure uniform distribution of sand. Figure 3.13 shows the weighing of the wooden box that is filled with sand.

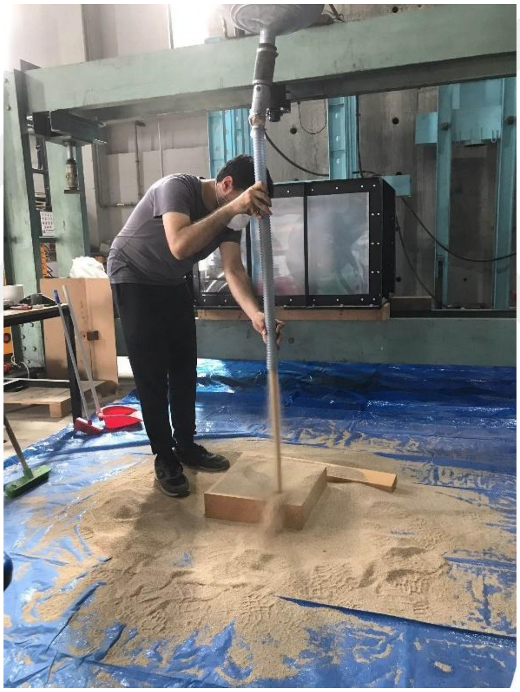

Figure 3.13. A photo depicting sand placement into the wooden calibration box using pluvation technique.

Figure 3.14. Weighing process of the wooden box filled with sand.

To obtain the minimum D_R, sand was poured into the wooden box in accordance with ASTM D4254-16. During sand pouring, a fixed pluviation height, consistent valve opening, and uniform pacing were maintained to achieve the desired uniformity in the sand layer. Multiple tests were conducted at various pluviation heights, and valve openings to establish a reliable calibration curve. The experimental results demonstrated that both sand raining density and pluviation height are critical parameters in achieving the desired D_R within the model tank, as expected. The required values for the pluviation parameters were obtained from these calibration tests. Figures 3.14.a and 3.14.b show the plots of pluviation height versus D_R, based on the data collected with pluvation calibration.

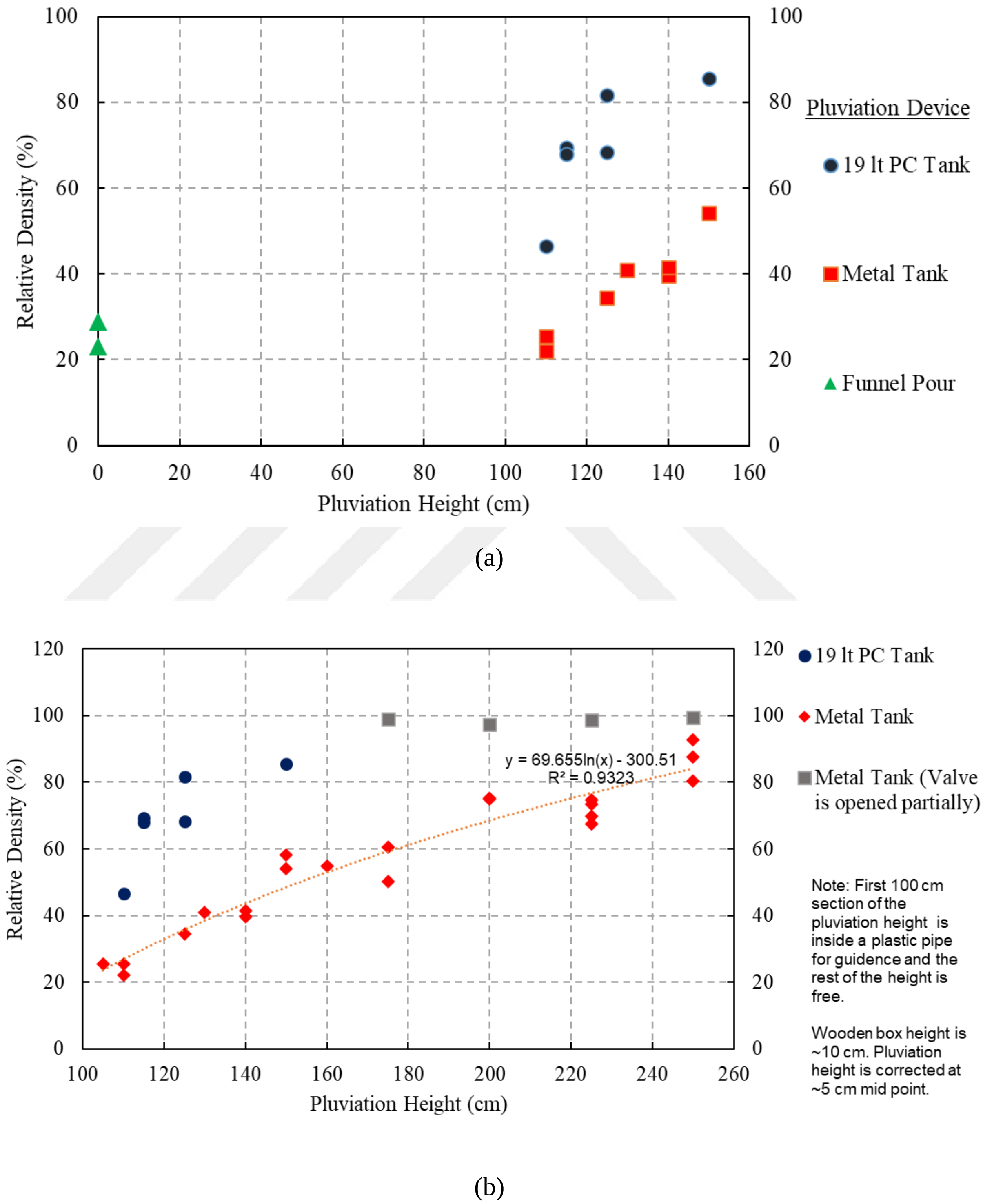

Figure 3.15. Pluviation height versus D_R: (a) rough calibration using various sand container devices, (b) detailed calibration for 19lt PC tank and metal tank with varying valve opening.

The results show that the pluviation data obtained from the metal tank follow an almost logarithmic trend, indicating that beyond a certain threshold, further increases in pluviation height do not change D_R. Accordingly, metal tank was utilized for placement of the sand in the model tank using the pluviation technique. The grey data represents the metal tank with the valve opened partially. These points tend to cluster around D_R = 100%, indicating that partially opening the valve results in higher and more consistent D_R values. From the calibration test results, when the valve is partially opened, the sand exits through a restricted area. This results in an increase in the velocity of individual sand particles due to the principles of fluid dynamics. Despite this higher particle velocity, the overall mass flow rate is reduced because the restricted opening limits the total amount of sand passing through per unit of time. In conclusion, the observed difference in D_R, can be interpreted as: the controlled discharge has a significant impact on how the sand particles settle. The overall flow of sand particles exiting at lower velocity tends to reduce turbulence during deposition, allowing the particles to interact and rearrange more efficiently as they settle. In contrast, when the valve is fully opened, the sand flows out at a much higher mass flow rate. While the individual particle velocity may not increase significantly, the larger volume of sand exiting all at once creates a more chaotic deposition environment. The rapid discharge often leads to turbulent interactions among particles, preventing them from settling in an orderly manner. This turbulence, combined with the bulkier nature of the flow, results in a loose packing with more void spaces, leading to a lower D_R.

3.12. Sand Placement in Model Box

The experimental procedure began with determining the thickness of sand layers in the model test tank, as shown in Figure 3.15. Colorful stickers were marked on the plexiglass surface at 10 cm intervals. This helped in accurately measuring the thickness of each sand layer and adjusting the level of the sand surface throughout the experiments. For each layer, the required soil mass was calculated based on density tests and the targeted D_R. Initially, the first 35 cm of the soil layer at the bottom of the tank was constructed using sand placed at D_R= 95%. The sand for each layer was carefully poured in 5-cm –thick lifts in accordance with the calibration test results, ensuring a flat and uniform sand surface.

Figure 3.16. The plexiglass side-view of the physical model test tank with layer markings.

After placing the bottommost 35 cm-thick sand layer, an additional 15 cm of sand was placed with the same relative density (D_R) as that to be used in the slope. After this stage, the wooden mold was placed to create the slope geometry. The mold's position was carefully aligned so that the local loading plate would be placed exactly at the edge of the crest. As the volume requirements varied for each mold segment, the precise amount of sand was weighed to achieve the desired densities calculated. The required sand mass for each 5 cm –thick lift (g) for the target densities in this research is shown in Table 3.4. The surface of the slope was then leveled and adjusted to ensure it was flat and horizontal. The surface level controls were performed using a spirit level.

Table 3.4. Estimated required sand mass for various target D_R .

Target D_R (%)	**95**	**70**	**40**
Target Void Ratio (e)	0.58	0.65	0.74
Target Dry Unit Weight of Sand γ_{dry} (kN/m^3)	16.41	15.72	14.96
Required Sand Mass for each 5 cm –thick lift (g)	90,340	86,520	82,340

Note: G_S=2.65, γ_w=9.81 kN/m^3.

3.13. Loading Frame, Instrumentation and Data Acquisition

The laboratory tests were carried out in the Structural Engineering Laboratory located on Boğaziçi Kandilli Campus using a loading frame equipped with a hydraulic jack. Load and deflection sensors were connected to the hydraulic jack to monitor displacements and load during testing. With a load capacity of up to 10 tons and a displacement range of 20 cm, the system required careful adaptation of the load application to the specific experimental needs. To achieve this, an additional apparatus was designed to adjust the application point of the load, ensuring precise alignment with the test setup. Furthermore, the loading rod was extended using stainless steel, chosen for its durability and resistance to deformation under high loads. Figure 3.16 shows the hydraulic jack, loading frame and loading rod. For the data acquisition, an additional control box was connected to transfer the collected data to the laboratory's main box, which was linked to a computer via an ethernet cable for real-time monitoring and operation.

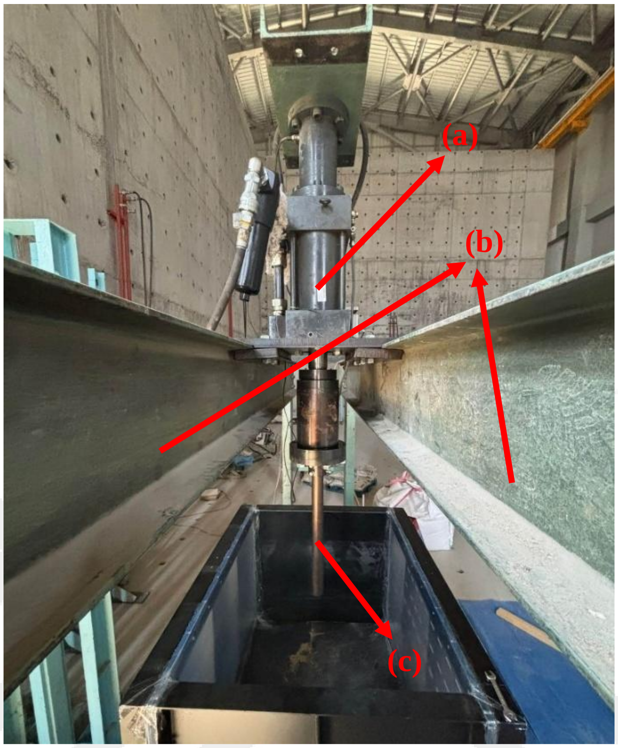

Figure 3.17. Loading system components: (a) hydraulic jack, (b) loading frame, (c) loading rod attached to loading plate.

The loading system utilized a hydraulic jack was controlled via the Testlab Control-Servo Hydraulic Control Software. This software provides flexibility to the user to perform either displacement-controlled tests or loading-controlled tests. In this study, displacement-controlled tests were performed. Using a hydraulic jack, the loading plate was moved vertically at a constant rate of 0.1 mm/s. During the tests, the software displayed both displacement and load in real-time through graphical outputs, enabling continuous monitoring and verification of the system's performance. Figure 3.17 (a) and (b) show the photos of TestBox and Testlab Control-Servo Hydraulic Control Software interface.

(a)

(b)

Figure 3.18. Data acquisition system: (a) testbox (b) Testlab Control-Servo Hydraulic Control Software interface on the computer.

To acquire data from the Testlab Control system, an additional TESTBOX Bridge was connected to the computer via USB. The bridge enabled the communication between the hardware and software. The Testlab Basic Configuration Software was employed to calibrate the TESTBOX, during which additional virtual channels were defined to accommodate specific experimental needs. For each experiment, a unique name was assigned within the software, ensuring organized data management. To synchronize data acquisition with the Testlab Control system, Testlab Basic Software was used to select and retrieve data for each experiment in real time. The program offered various time intervals for data extraction, including 0.125 s, 0.25 s, 0.5 s, and 1 s. To minimize excessive data while maintaining sufficient accuracy, a 0.5-second interval was selected for this study. The data, exported in text format by the Testlab Basic Software, was processed and used.

3.14. Experimental Setup and Measurements

For tests involving piles, additional steps were included to experimental setup to ensure accurate pile placement and stability. Piles were embedded into very dense sand layers with D_R= 95%. Approximately 40% of their total length was socketed into this very dense region. To prevent pile movement or tilting during sand placement, a stabilizer was attached to the model tank before sand placement. Piles were connected to the pile placement apparatus and checked with a spirit level. Figure 3.17(a) shows the pile placement apparatus and pile arrangement. Pile group length was determined as such a minimum of 1.5 times the loading plate length was covered in the slope during loading. The position of the pile heads was arranged such that the heads of the piles are located on the upper part of the slope near the crest. After completing the placement of the dense sand with D_R=95% in the socketed zone, the pile placement apparatus was removed carefully as illustrated in Figure 3.18(b). Then the same procedure for the construction of slope surface was carried out similarly to those previously described for natural slopes (without piles).

(a)

(b)

Figure 3.19. Photo depicting the placement of piles in the slope model: (a)top view, (b)side view

The vertical displacement and vertical applied load measurements were collected on the top of the loading plate using the Testlab Basic Software. Additionally, two (2) 24-megapixel cameras and a video recorder were used to observe and document the deformation throughout the test. The cameras captured raw-format photos at one-second intervals to ensure high-resolution imagery for detailed analysis, such as PIV, to be conducted later. To maintain consistent lighting exposure, two (2) light projectors were positioned above the loading frame. Additionally, several laser transducers were placed at holder locations within the tank to record the pile head displacements during the tests. Figure 3.19 shows the pile arrangement at the end of the slope erection before the application of the load. The entire test setup configuration is shown in Figure 3.20.

Figure 3.20. Experimental test setup with piles.

Figure 3.21. Experimental Setup (a) local loading plate, (b) model tank, (c) piles, (d) hydraulic jack, (e) camera 1, (f) camera 2, (g) control box, (h) loading frame.

4. MODEL TESTS RESULTS ON LOCALLY LOADED SLOPES AND LOCALLY LOADED SLOPES STABILIZED WITH PILES

In content of this Thesis, a series of laboratory experiments were performed on the small-scale slope models. The detailed results of these tests are presented in this Chapter.

4.1. Experimental Plan

An initial laboratory test was conducted on level ground to better understand the load – settlement response of the sand constructed with D_R = 40%. An attempt was made to calculate the subgrade reaction modulus from this test performed at level ground ($\beta = 0^\circ$). Then, locally loaded slopes with $\beta = 30^\circ$ constructed with sand prepared at D_R = 40% and D_R = 70% were tested. One (1) additional test was performed on the slope model with $\beta = 30^\circ$ constructed with D_R = 40% to see the repeatability of the results. The last test was performed on the slope model in which a group of five (5) piles were introduced to observe the effects on stability. Five (5) tests were performed using a local loading plate under a displacement-controlled loading rate of 0.1 mm/s. Table 4.1 summarizes various configurations and parameters for the tests performed on locally loaded sandy slopes.

Table 4.1. Small-scale physical model test plan.

Test Number	Loading Plate	β	D_R	Number of Pile	Loading Rate
1	Local	0˚	40%	None	0.1 mm/s
2	Local	30˚	40%	None	0.1 mm/s
3	Local	30˚	40%	None	0.1 mm/s
4	Local	30˚	70%	None	0.1 mm/s
5	Local	30˚	40%	5	0.1 mm/s

4.2. Data Reduction

This section outlines the methodology for data reduction based on the example results of the tests performed on a slope with $\beta = 30^\circ$ and $D_R = 40\%$ (Test No.2) as presented in Table 4.1. The raw data obtained from the experiments shows that for a long period of time, even though displacement of the loading plate increases, and the corresponding applied load does not pick up. This is likely due to the fact that the plate is not in complete contact with the sand at the start of the test. In data reduction phase, the data was corrected for this initial displacement measurement corresponding to the point of initial load increase, thereby establishing a zero-load reference point was established. Subsequently, stress values corresponding to the applied load were calculated. The initial stress values remain at zero until the plate contacts the sand. Then, both displacement and stress values increased slowly. In most cases the initial portion of the plot showed curvilinear characteristics due to issues with surface leveling of the sand. When needed the initial curvilinear portion of the data was also refined. The corrected data was generated accordingly, as illustrated in Figure 4.1.

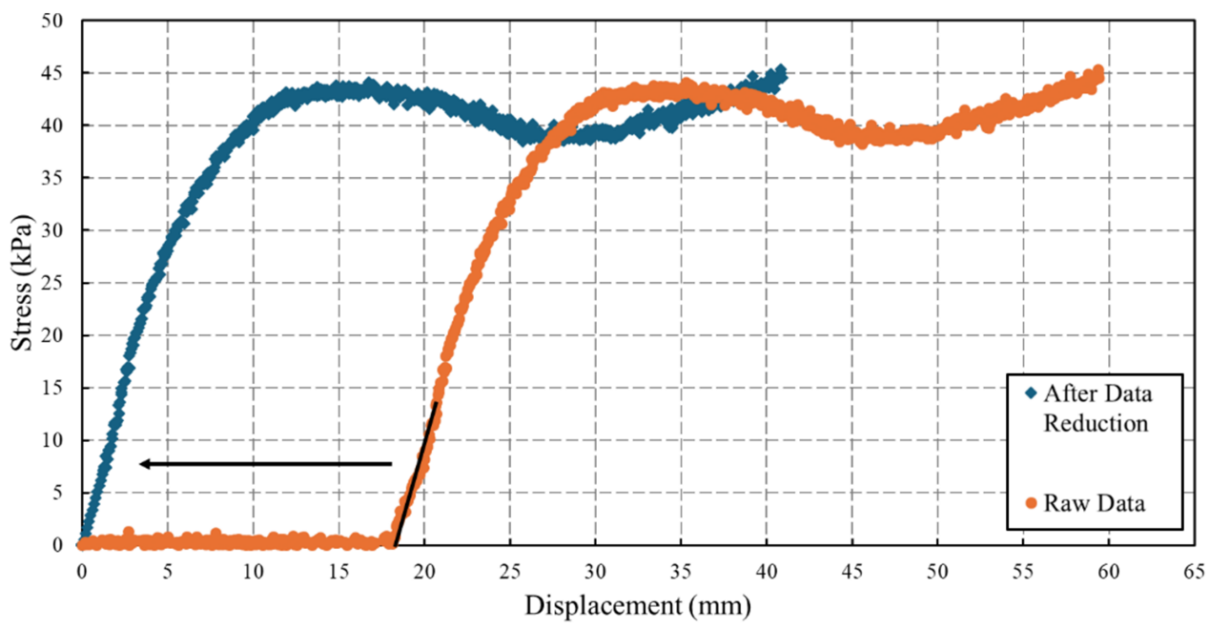

Figure 4.1. Example vertical displacement versus vertical stress of the loaded slope: data reduction.

4.3. Test Results of Locally Loaded Sand with β=0˚ and D_R =40%

This test was performed on the level ground aimed to back-calculate the subgrade reaction modulus (*k*) of the sand. The test was performed on sand with β =0˚ (level ground condition) and D_R =40% loaded with an area of 12.5 cm by 25 cm. This test corresponds to Test No.1 in Table 4.1. The load was increased with a displacement rate of 0.1 mm/s and vertical displacement of the plate was measured. The graph presented in Figure 4.2 illustrates the relationship between vertical displacement of the plate (mm) and stress on the loading plate (kPa).

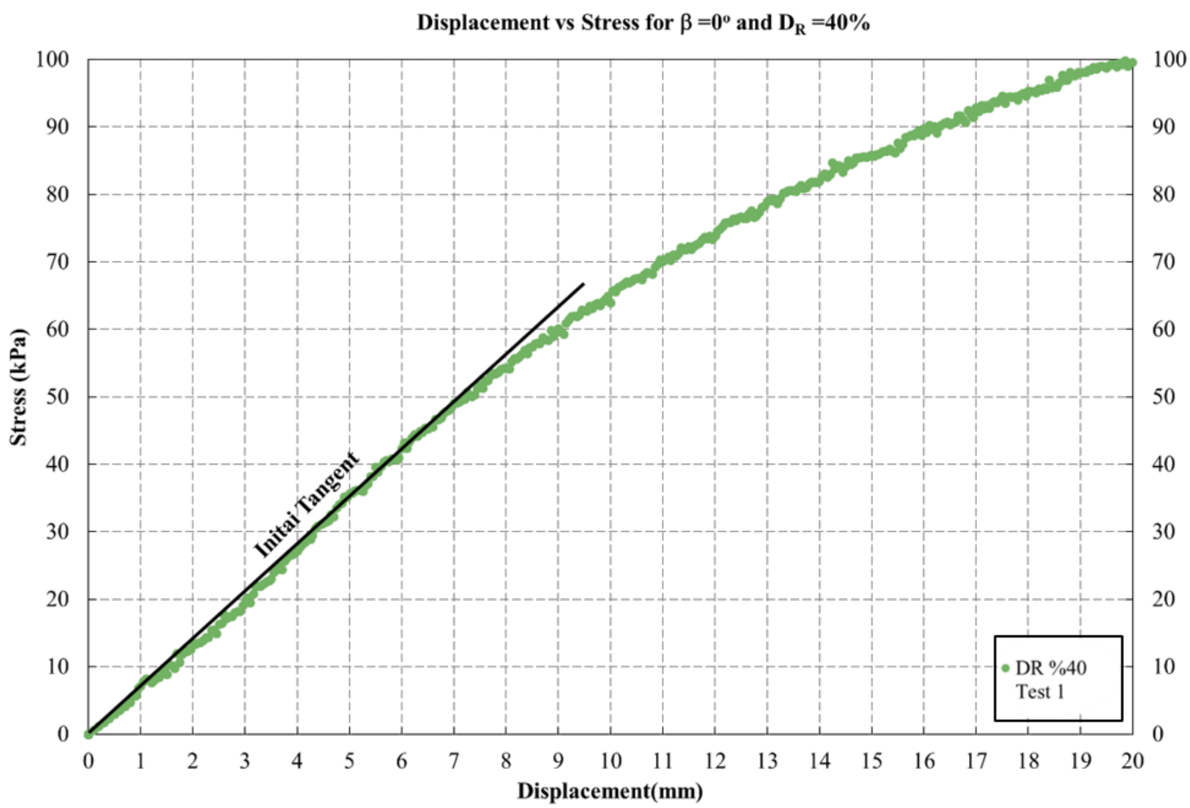

Figure 4.2. Vertical displacement versus vertical stress plot of the locally loaded sand with β = 0˚ and D_R =40%.

The displacement-stress curve reveals a consistently increasing trend, indicative of the progressive resistance of soil under the applied load. The linearity of the curve in its very early stages suggests an elastic response of the soil, where deformation is proportional to the applied stress. As the stress increases, the slope of the curve begins to decrease slightly, which could be explained as a transition into a nonlinear response phase as the plastic behavior dominates.

An initial attempt was also made to estimate the subgrade reaction modulus (*k*) of the sand tested at D_R =40%. *k* is defined as the slope of the displacement-stress curve based on elasticity theory as stated in equation (4.1). Different methods, such as the tangent modulus and secant modulus, can be used to determine the *k* value. Subgrade reaction modulus (*k*) can be represented as,

$$k = \frac{q}{\delta} \tag{4.1}$$

where q is vertical stress (kPa), δ is displacement (m) (Hudson and Siddiqi, 1970). From the load- settlement plot of this experiment performed on level ground, the initial tangent modulus was calculated as 7,132 $kN/m^2/m$. This calculated k value is somewhat lower than the range reported for medium-dense sands, it falls within the range reported for loose sands (Bowles, 1996). One possible explanation is that the subgrade reaction modulus, *k*, depends on the plate area (Briaud, 2007). In this experiment, the plate used measured 0.125 m × 0.25 m, and such small plates can lead to unreliable data, as demonstrated by Teodoru and Toma (2009). This is likely to be the main reason for this relatively lower value. Furthermore, in field plate load tests, a portion of the soil is typically removed, and test is performed at a depth to ensure proper contact between the plate and the ground. However, this procedure could not be performed in this experiment performed in the laboratory, which may have affected the results. Additionally, plate load tests are usually conducted *in situ* where stress levels are higher than those achievable under laboratory conditions. Finally, the soil in this experiment is nearly pure sand, which differs from the typical field conditions, as field tests are generally not conducted in pure sand environments. Lastly, the surficial sand density is generally low due to disturbances. All these factors likely contributed to the relatively lower *k* value, and this discrepancy warrants further investigation.

4.4. Test Results for Sandy Slope with β=30˚ and D_R =40%

Two (2) tests were performed for a slope with β=30˚ and D_R =40% loaded using the same local plate presented in Test No.1. These tests correspond to Test No.2 and Test No.3 in Table 4.1. Vertical displacement was applied again at 0.1 mm/s. Both tests were carried out with the same slope conditions (β=30˚ and D_R =40%). Accordingly, the uniformness and consistency of sand placement, and the reliability of the measurement system were assessed through this test repeatability check. Figure 4.3 shows the vertical displacement of the loading plate versus vertical stress obtained from these two (2) identical tests.

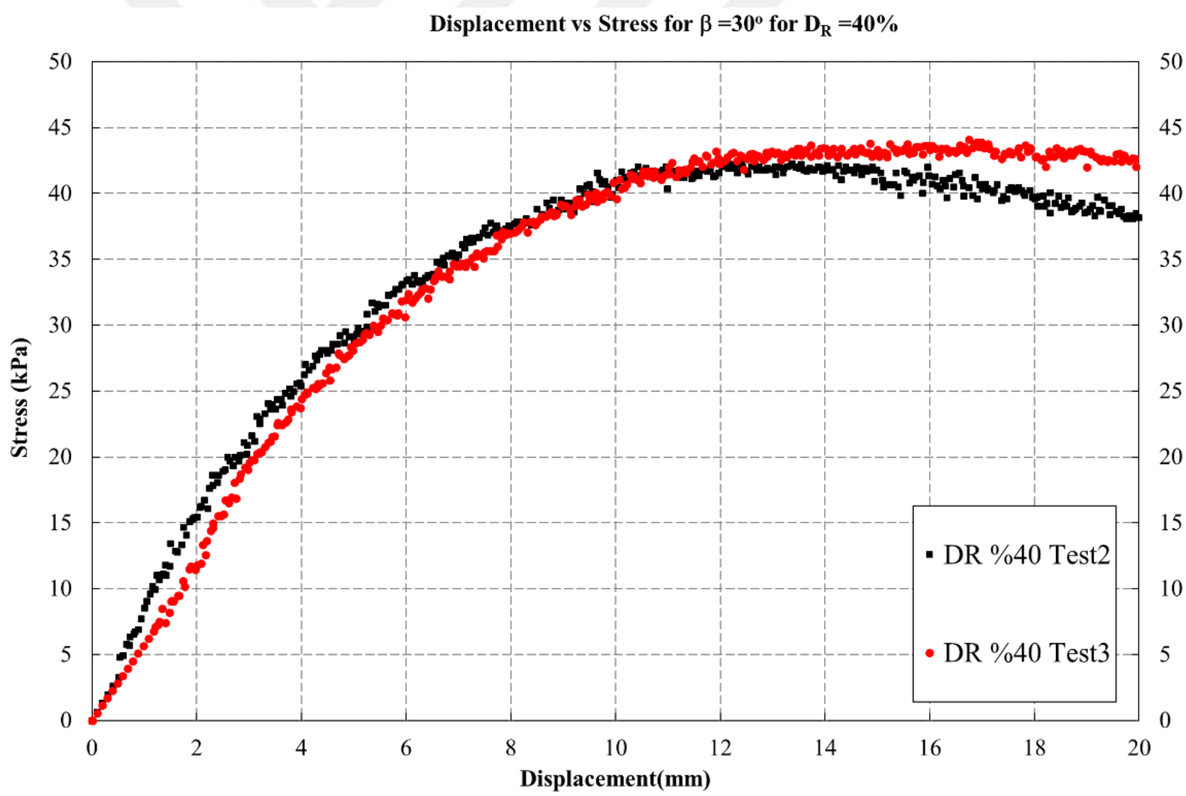

Figure 4.3. Vertical displacement versus vertical stress plot of the locally loaded slope with β = 30˚ and D_R =40%.

The progression of the load response from a steep incline to a more gradual slope after 5 mm of displacement suggests a transition from elastic to plastic behavior in the soil. Initially, the soil behaves linearly under small strains, but as the strain increases, it begins to deform without showing resistance. This characteristic of the response was observed in both test results. The peak stress values reached in both tests were quite close to each other (≅45 kPa). This result shows the reliability of the test setup and the measurement system as well as repeatability of the tests. The slope withstands stresses up to a threshold value, beyond which, stresses start to drop with an increase in displacements, indicating failure.

Figure 4.4 compares results of the tests conducted with β = 30˚ with those performed with β = 0˚ (level ground) for D_R= 40%. The results show that existing slope results in noticeable changes in vertical displacement-vertical stress behavior compared to the β = 0˚ (level ground) condition. Initial part of the curves for tests performed with β = 30˚ (Test No.2 and Test No.3) follow a similar trend with the case with β = 0˚ (level ground), that is the Test No.1. However, as stress increases, the tests performed with β = 30˚ show significantly higher displacements than the level ground case (β = 0˚) for the same stress levels. The loss of bearing capacity and slope stability is expected, as the failure planes do not have any resistance on one side of the plate for β = 30˚ cases. As the loading increases, β = 30˚ cases begin to deviate more quickly than β = 0˚ (level ground) case, which continues almost linearly. This suggests that the slope causes the soil to deform more easily under higher stresses, due to the reduction in resistance to the load caused by the sloped geometry.

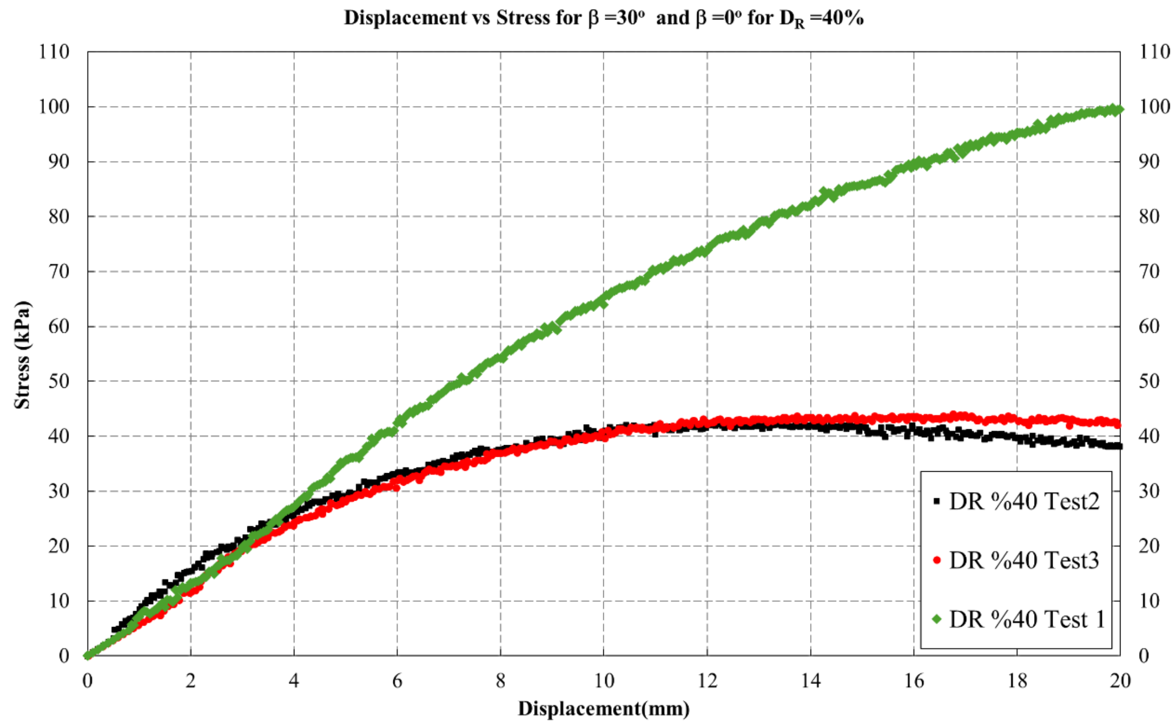

Figure 4.4. Vertical displacement versus vertical stress plot of the locally loaded slope with β = 30˚ (Test No.2 and Test No.3) and locally loaded sand β = 0˚ (level ground; Test No.1) and D_R =40%.

Photographs were taken from both the face (front-view) and the side (side view) of the slope, to investigate the failure shape. Figure 4.5 (a) and (b) show these deformed shapes based on front-view and side-view pictures. A 3D failure shape, that resembled a stress bulb was clearly observed. The load distribution extended beyond the loading plate, and the corresponding failure shape was clearly visible. The deformed shape after loading, curving outward from beneath the plate, also suggests how the failure expands, with stress being highest directly under the load. 3D failure shapes were observed on these locally loaded slopes, highlighting the importance of 3D modeling in laboratory tests and numerical analysis.

(a)

(b)

Figure 4.5. Photos depicting displacements in soil after loading: (a) front-view of slope surface (b) side-view of slope surface.

In conclusion, the close alignment of the load response curves from both tests at D_R= 40% confirms the reliability of the experimental methodology, which is essential for physical small-scale model tests.

4.5. Test Results for Sandy Slope with β=30˚ and D_R =70%

Another test is performed for a slope with β=30˚ and D_R =70% (Test No.4 in Table 4.1), while keeping all other conditions the same as the case with β=30˚ and D_R =40% (Test No.2 in Table 4.1). Figure 4.6 shows the vertical displacement versus vertical stress relationship of the loading plate for these cases with slopes with different D_R values. As expected, the test with D_R= 70% exhibits a higher peak stress compared with the case with D_R= 40%. In contrast, the test with D_R =40% demonstrates a more gradual increase in stress and does not exhibit a clear peak, suggesting more ductile behavior under the same loading conditions. However, beyond the peak stress value for the D_R = 70%, vertical stress decreases and converges to those observed in the case with D_R= 40%.

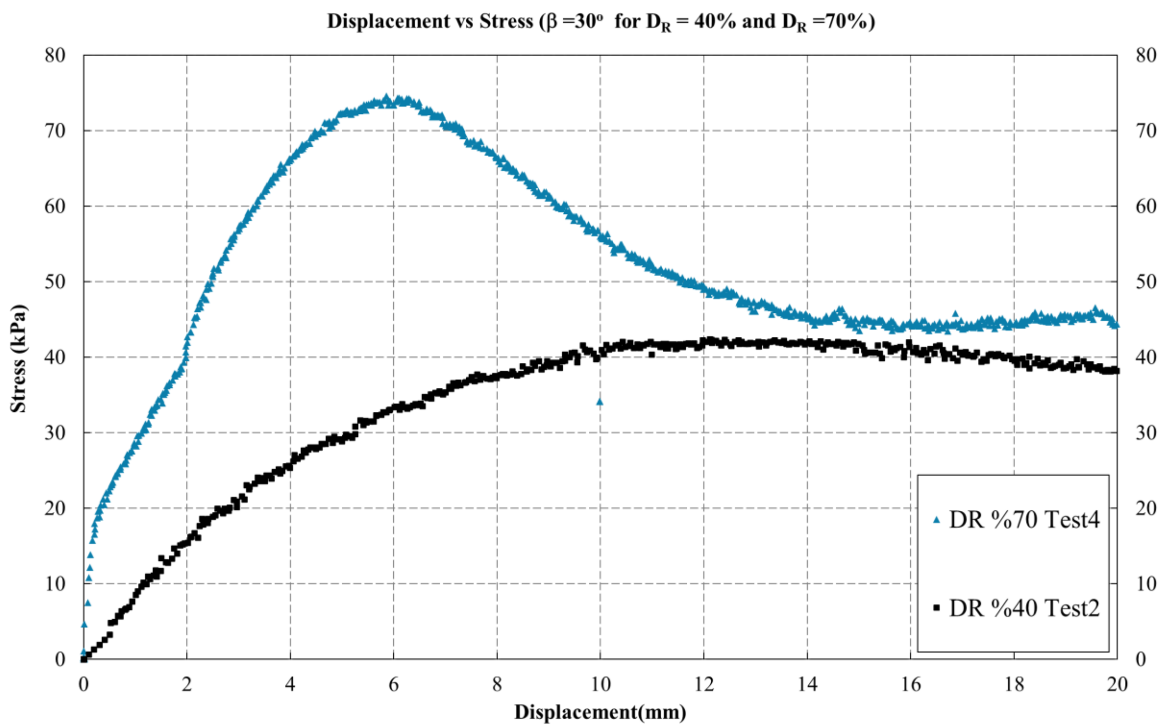

Figure 4.6. Vertical displacement versus vertical stress plot of the locally loaded slope with β = 30˚ with D_R =40% (Test 2) and D_R =70% (Test 4).

As D_R increases the particle interlocking also increases, leading to greater stiffness and strength at small displacements. This is reflected in the steeper initial slope of the load response curve for the D_R= 70% (Test No 4). In contrast, the test with D_R= 40% (Test No.2) shows significant vertical displacement even at low stress levels, suggesting a weaker interparticle resistance. These two (2) results also resemble the results of a shear test performed on a dilative and contractive sand specimen in a triaxial test, both merging at higher strain levels at ultimate states. This behavior emphasizes that D_R controls the deformation and failure characteristics of sandy slopes.

4.6. Test Results for Sandy Slope with β=30˚ and D_R =40% Stabilized with Piles

To evaluate the impact of pile stabilization on sandy slopes, a final test was conducted for a slope with β=30˚ and D_R =40% corresponding to Test No.5 in Table 4.1. Piles were installed near the crest of the slope. The cover area was selected slightly greater than 1.5 times the loading base length (1.5l, where l = 25 cm), while the spacing- to-pile-diameter ratio (s/d_p) was set to three (3) for the center three (3) piles corresponding to the alignment of the load. However, due to construction constraints, the piles at the left and right ends of the group, the outermost two piles were placed with slightly reduced spacing, approximately with 2.6d_p. All in all, as the coverage length of this pile row was deemed sufficient, and the slightly reduced spacing at the ends was considered as a minor deviation. All other test conditions were kept the same as Test No.3. Figure 4.7 compares the vertical displacement versus vertical stress plots for the locally loaded slopes and the locally loaded pile-stabilized slopes with β=30˚ and D_R =40%.

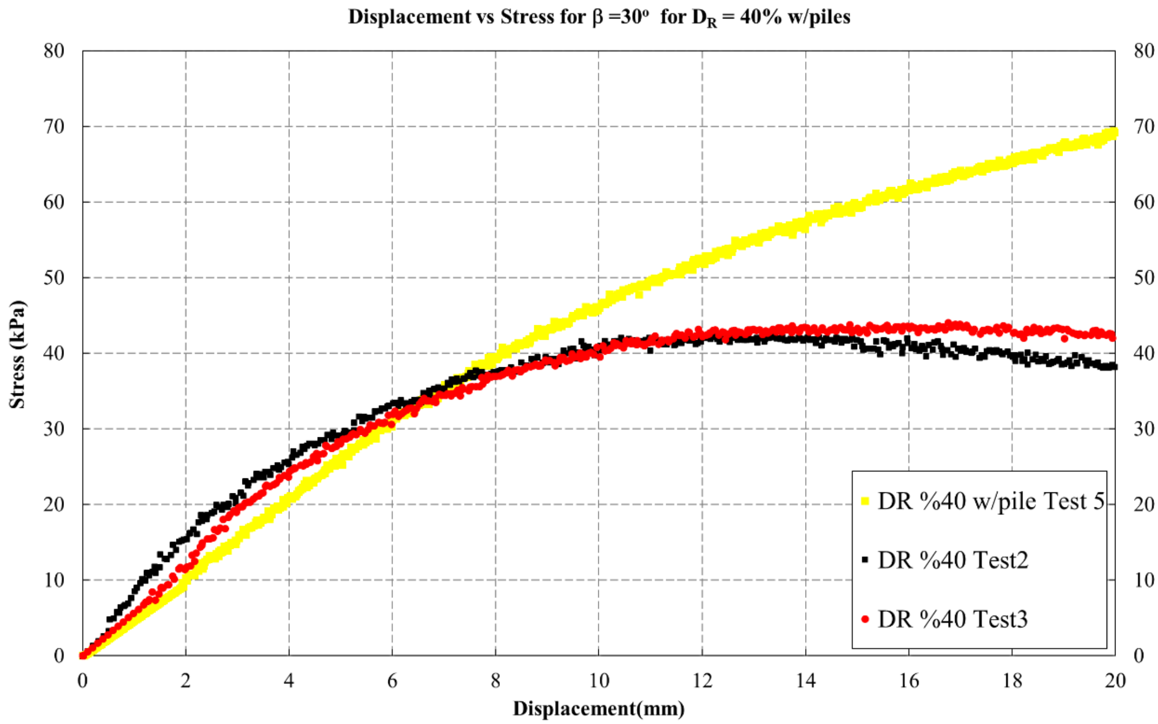

Figure 4.7. Vertical displacement versus vertical stress plot of the locally loaded slope and locally loaded slope stabilized with piles (slope with β = 30˚ and D_R =40%).

From the graph in Figure 4.7 it is evident that pile stabilization significantly improves the stability and deformation resistance of the slope. The slope stabilized with pile exhibits higher stress values for the same displacement levels compared to the natural slope. Notably, the stabilized slope maintains a more consistent upward trend, reaching higher stress values at approximately the same displacement levels. On the other hand, the curve for the slope that is not stabilized with piles, levels off at around 45 kPa. This clearly demonstrates how much the piles enhance the slope stability. The improvement in stress-bearing capacity of the stabilized slope, can be attributed to the piles' ability to form an arching mechanism, causing a redistribution of the stress within the slope-pile system. Slope's resistance against deformation shows that arching is activated in the pile group and the pile row acts as barrier against soil movement.

To see how the load capacity of the pile stabilized slope would be compared with locally loaded sand with level ground (β = 0˚); Test No.1 and Test No.5 with D_R =40% in Figure 4.8. During the loading test on level-ground case, the stress reaches a level of 100 kPa. However, in the case where the slope is supported with piles, the stress is approximately 70 kPa at the same displacement. It is clearly seen that even with pile-stabilization load carrying capacity of the slope is less than the case with level ground.

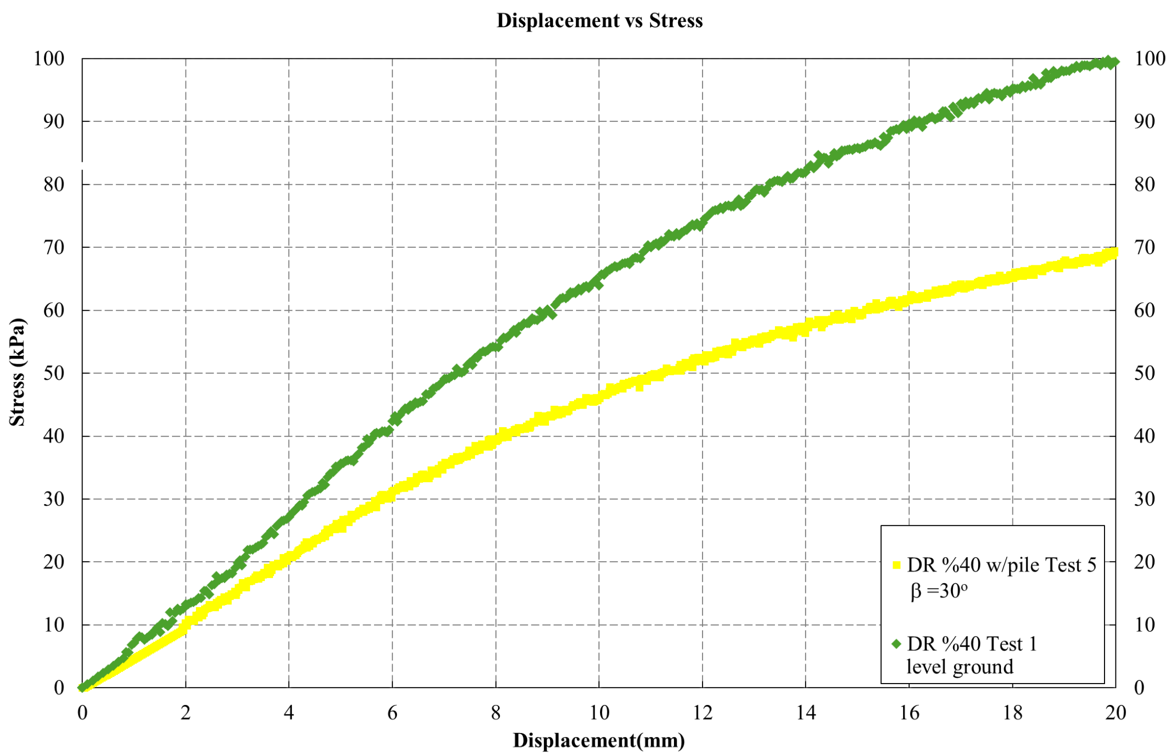

Figure 4.8. Vertical displacement versus vertical stress plot of locally loaded sand β = 0˚ (level ground; Test No.1) and locally loaded slope stabilized with piles (β = 30˚; Test No.5) with D_R =40%.

Figure 4.9a and Figure 4.9b, depict two (2) images that were taken before and after loading for locally loaded slope stabilized with piles (β = 30˚; Test No.5) with D_R =40%. These images illustrate the pile arching effect observed during loading on the pile-stabilized sandy slope. After loading, noticeable pile-head displacements occur, without significant soil displacements in between the piles. This result indicates the development of an arching mechanism in between the piles. Through arching, the applied load was transferred from the soil to the piles. Another observation is the arch-like shape of the pile row with the maximum displacement at the center. As can be seen in Figure 4.9b, the horizontal displacement of the centermost pile was the maximum and measured as 37 mm. The displacements of the outermost piles were the least among the pile group due to the stress distribution behavior. Table 4.2 presents the horizontal pile-head displacements measured for all five (5) piles in the row based on images captured before and after loading. Pile No.1 and No.5 are the outermost piles, and Pile No.3 is the central pile (see Figure 4.9).

Table 4.2. Horizontal displacement of pile head.

Pile Number	Horizontal Displacement of Pile Head (mm)
1	12
2	20
3	37
4	21
5	12

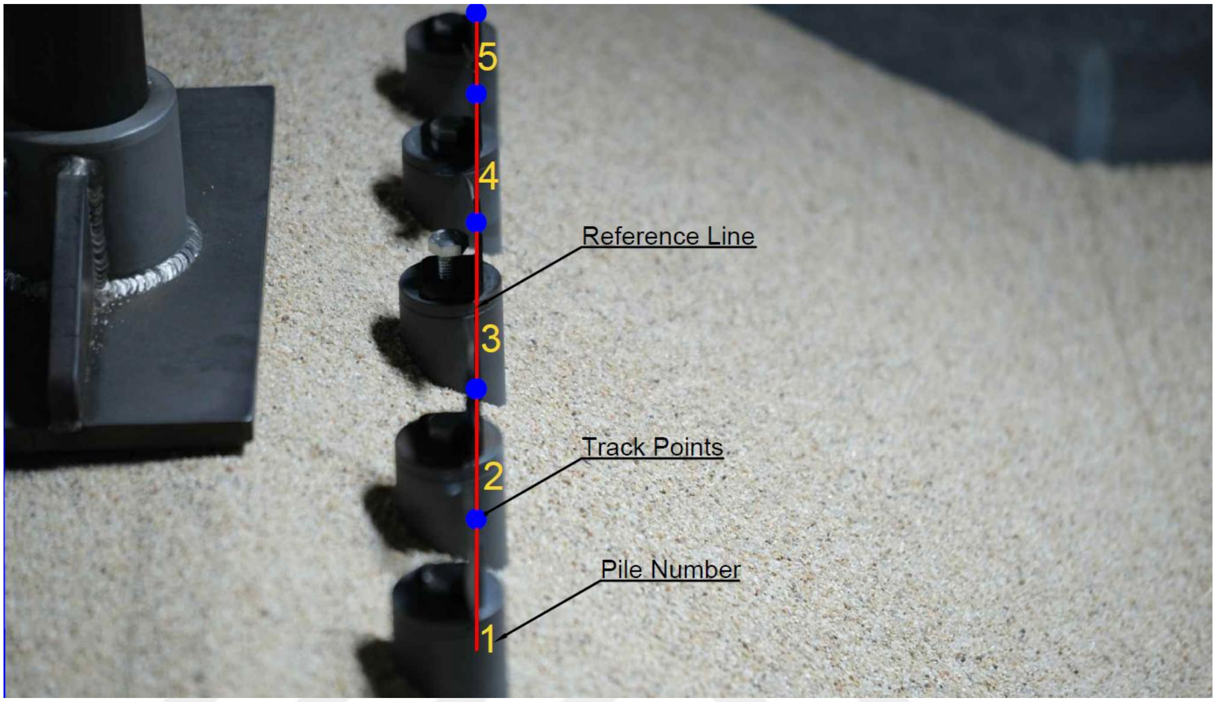

(a)

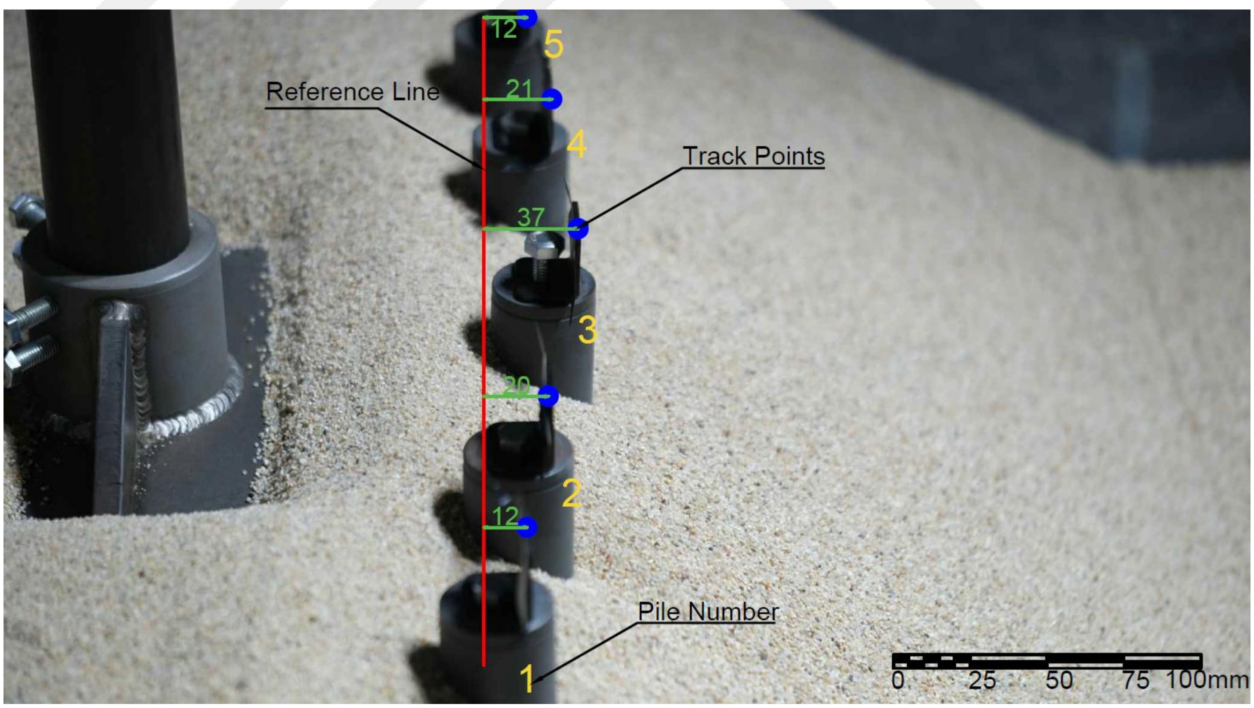

(b)

Figure 4.9. Photos depicting pile head displacements in the pile-stabilized slope with β=30˚ and D_R =40%: (a) before loading and (b) after loading.

5. COMPARISON OF EXPERIMENTAL RESULTS WITH 3D NUMERICAL ANALYSIS

This section presents the attempts to compare the experimental results with the numerical analysis performed using Finite Element Method (FEM) through Plaxis 3D software. The material properties, including those of the pile, soil, and plate, were carefully selected to reflect the conditions in the laboratory. The loading process was carefully simulated such that it is consistent with the experimental setup. Finally, the comparison section discusses how well the FEM results align with the experimental data, highlighting any observed differences and discussing possible reasons for these variations.

5.1. Numerical Methodology

Selecting an appropriate material model in Plaxis 3D is crucial to ensuring accurate and reliable predictions. The accuracy of FE analyses largely depends on the constitutive models used to describe material behavior under various loading conditions. Plaxis 3D provides a wide range of well-known soil constitutive models, including simple linear elastic models, Mohr-Coulomb (MC) models, hardening soil (HS) models, hardening soil models with small strain stiffness (HSS). Among these, the hardening soil (HS) model was chosen for its advanced capabilities in simulating the stiffness behavior. The Hardening Soil (HS) model is an advanced approach to simulating soil behavior, designed to account for the stiffness changes in soils that deform under the effect of various loads. Unlike simple elastic perfectly-plastic models, in which the yield surface remains fixed in stress space, the HS model uses hardening plasticity. The yield surface expands as the soil undergoes permanent deformations. Shear hardening, which models the permanent deformation caused by shear forces during compression hardening, was considered in this model. The required input parameters for the HS model are presented in Table 5.1.

Table 5.1. Required input parameters and their symbols in HS models.

Required Input Parameter	Symbol
Effective cohesion (kPa)	c'
Void ratio	e
Effective angle of friction (Degree)	ϕ'
Dilatancy angle (Degree)	ψ
Reference stiffness modulus corresponding to the reference confining pressure p^{ref} (kPa)	E_{50}^{ref}
Plastic straining due to primary compression(kPa)	E_{oed}^{ref}
Elastic unloading/reloading (kPa)	E_{ur}^{ref}
Stress-dependent stiffness according to a power law	m
Poisson ratio	v_{ur}
Failure ratio	R_f
Reference stress for stiffness (kPa)	p^{ref}

The power m value, Poisson's ratio, and failure ratio are set to their default values, which are 0.5, 0.2, and 0.9, respectively. To estimate the *E* values to be used in HS model, Brinkgreve et al. (2010) recommends the following *E* formulas:

$$E_{50}^{ref} = 60000 \times \frac{D_R}{100}\left(\frac{kN}{m^2}\right), \tag{5.2}$$

$$E_{oed}^{ref} = 60000 \times \frac{D_R}{100}\left(\frac{kN}{m^2}\right), \tag{5.3}$$

$$E_{ur}^{ref} = 180000 \times \frac{D_R}{100}\left(\frac{kN}{m^2}\right). \tag{5.4}$$

These formulas, as discussed by Brinkgreve et al. (2010), this is an empirical approach to estimate parameters of the HS. It is important to note that all of these correlations for the parameter *E* are calibrated for p^{ref} = 100 kN/m^2. *E* values to be used in the numerical analysis were computed using the correlations listed above.

To determine sand friction angle and dilatancy angle of sand at D_R= 40%, D_R= 70% and D_R= 94%, Bolton's (1986) equation was used. His work emphasized that the difference between the critical state strength and peak strength of sand are mainly influenced by the two states of sand: D_R and mean effective stress (p'). It should be noted that, Bolton's (1986) equations were derived separately for triaxial and plane strain conditions. Bolton's (1986) equations (5.5) and (5.6) were used to calculate ϕ_{peak} values. The ϕ_c was obtained 29.5° by conducting the simple test procedure proposed by Santamarina and Cho (2001), as previously explained in Chapter 3. The Bolton's equation can be expressed as follows,

$$I_R = I_D \times (Q - \ln p') - R, \tag{5.5}$$

$$\phi_{peak} = 3 \times I_R + \phi_c, \tag{5.6}$$

where, $I_D = \frac{D_R}{100}$; D_R is relative density; p' is the mean effective confining stress in kPa, Q and R are unitless soil constants determined based on grain characteristics and stress level; I_R is the relative dilatancy index that is expected to be in the 0 to 4 range (Bolton,1986). The stress state of each test presented in this thesis was different. All in all, considering the stress states of all the tests performed, the representative mean effective stress (p') to be used in Bolton's equation was selected as 50 kPa. The Q and R values corresponding to this relatively low mean effective confining stress were derived using the correlation proposed by Chakraborty and Salgado (2010). Using $\phi_c = 29.5°$ in Bolton's equation, the ϕ_{peak} values corresponding to D_R = 40% and D_R = 95%, were estimated as 33.5° and 43.1°, respectively (see Table 5.2). Using the correlations presented above, initial estimations of the soil parameters were made. Table 5.3 summarizes the soil model and the parameters adopted in the numerical analysis, selected based on the results of these correlations and informed engineering judgment.

Table 5.2. Estimated shear strength parameters by using Bolton's (1986) equations.

Target D_R (%)	95	70	40
Critical Angle (ϕ_c)	29.5°	29.5°	29.5°
Peak Angle (ϕ_{peak})	43.1°	38.8°	33.5°

Table 5.3. Input soil parameters.

Soil	γ_{dry} (kN/m³)	c' (kN/m²)	e	ϕ' (°)	ψ (°)	m	R_f	v_{ur}	E_{50}^{ref} (kN/m²)	E_{oed}^{ref} (kN/m²)	E_{ur}^{ref} (kN/m²)
Sand D_R = %40	14.96	1	0.74	33	3	0.5	0.9	0.2	24000	24000	72000

Sand D_R = %95	16.41	1	0.58	42	12	0.5	0.9	0.2	57000	57000	171000

A modulus of elasticity of 200 GPa and a Poisson's ratio of 0.3 were assigned to the loading plate, made of steel with a thickness of 0.1 mm Similarly, the pile, made of PVC, was modeled with a modulus of elasticity of 4 GPa and a Poisson's ratio of 0.41. Table 5.4. provides the material properties of pile and loading plate in Plaxis 3D.

Table 5.4. Input material properties of piles and loading plate in Plaxis 3D.

Material	Thickness(m)	v_{ur}	E (kN/m^2)
Loading Plate	0.01	0.30	200×10^6
Pile	0.005	0.41	4×10^6

5.2. 3D Model Configuration

The numerical modeling approach was developed to accurately simulate the interaction between the loading plate, the pile, and the surrounding soil. Figure 5.1 provides an illustration of the 3D numerical model and its dimensions. The model was prepared identical to the laboratory physical model. To achieve accurate stress and strain distributions, a fine mesh was employed in critical areas such as the interface between the pile and soil and beneath the loading plate. In regions distant from these critical areas, a coarser mesh was used to optimize computational efficiency and to reduce the calculation time. Figure 5.2(a) and Figure 5.2(b) show the mesh distribution of the locally loaded sandy slope and the locally loaded sandy slope stabilized with piles, respectively.

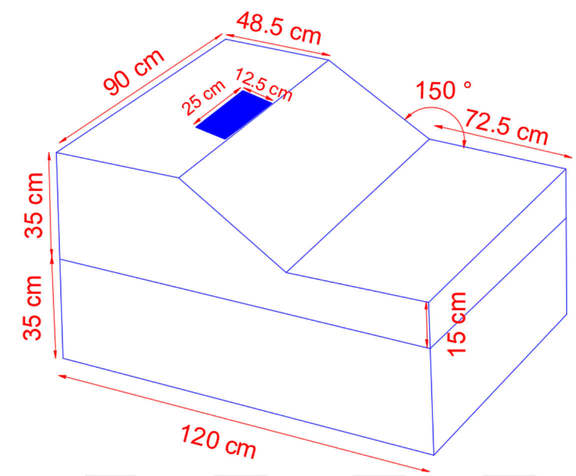

Figure 5.1. Model dimensions of the FE Model of locally loaded slope

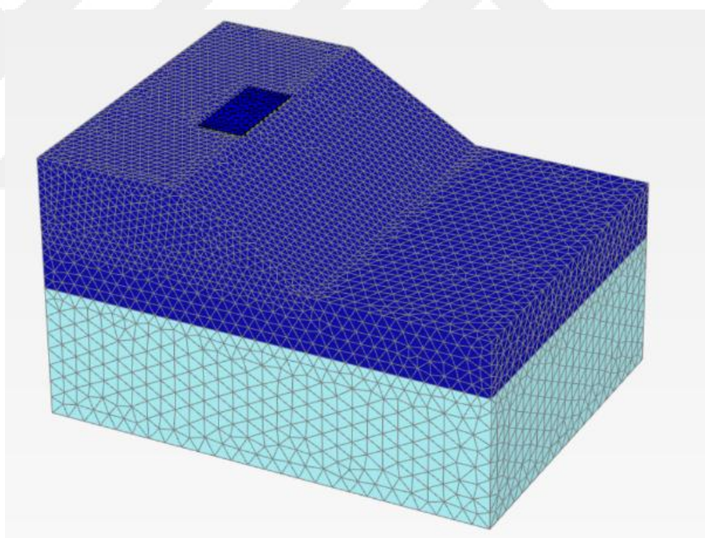

(a)

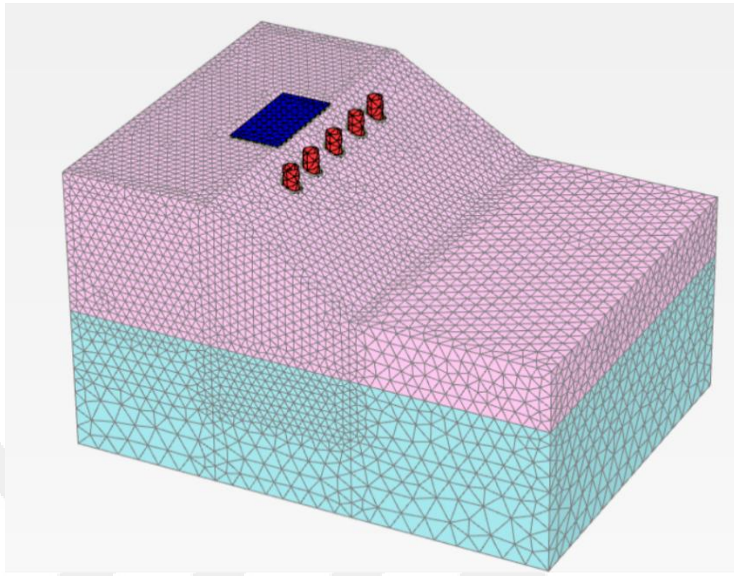

(b)

Figure 5.2. FE model and mesh of (a) locally loaded sandy slope, (b) locally loaded sandy slope stabilized with piles.

Interface elements are incorporated between the loading plate, pile, and soil to simulate frictional interactions. Pile materials suggested by Tekdemir (2023) were adopted for the volume piles. Loading parameters were carefully defined to reflect laboratory conditions of the displacement-controlled loading method. That is why, 20 mm prescribed displacement is defined on the plate element

5.3. Construction Stages

The first phase of the model was definition of the slope by gravity loading. This step was implemented to calculate the soil stresses resulting from the self-weight of the soil. Following this, a nill plastic phase was introduced. In this phase, displacements from the previous step were reset to zero while maintaining the calculated stresses. Subsequent phases of the analysis were based on the conditions established during the nill phase and progressed accordingly. The third phase is the activation of volume piles and interphase elements while deactivating the soils inside the piles, since the piles used in experiments are PVC pipes (hollow piles). The final phase of the model construction involves the activation of the loading plate, interphase elements, and prescribed displacements. Figure 5.3 illustrates the staged construction used in the Plaxis 3D models of pile-stabilized slopes.

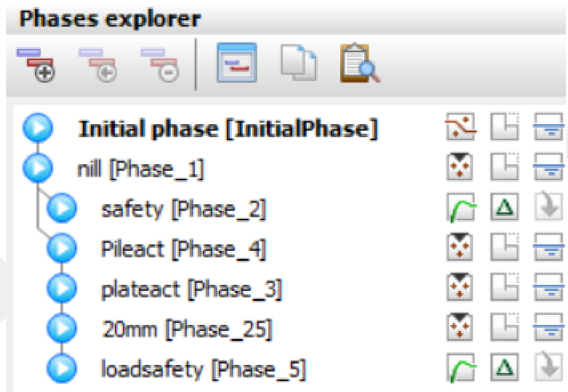

Figure 5.3. Construction stages for the sandy slope stabilized with piles.

5.4. Comparison of Numerical Analysis with Physical Model Test Results

The numerical analysis was performed for sandy slopes with D_R= 40%. To ensure that there is a reasonable comparison, data was extracted from the central node of the loading plate in the numerical model. Plaxis 3D provides the reaction force (F_z) and displacement values at the selected nodes. To align the comparison units with the experimental results, F_z was converted into stress values by dividing it by the area of the loading plate. An initial comparison was performed for the level ground case. Figure 5.4. illustrates the comparison of vertical displacement versus stress plots obtained from the small-scale physical model tests and the numerical analysis for β = 0˚(level ground) with D_R = 40% assuming an E=24 MPa for this medium dense sand.

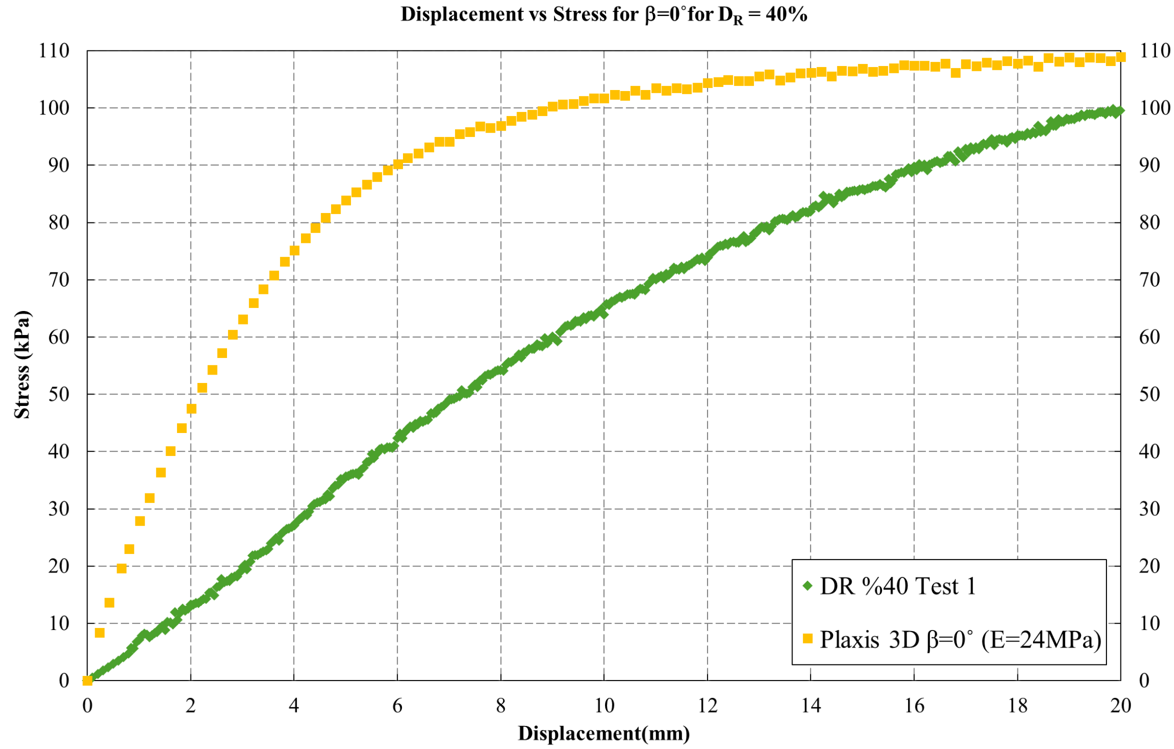

Figure 5.4. Comparison of experimental and numerical analysis results obtained for locally loaded sand with $\beta = 0^{\circ}$ (level ground) and $D_R = 40\%$.

For a given displacement, a clear difference was observed between the stress values obtained from the numerical and experimental results. However, the overall behavior and shape of the two (2) curves show a strong resemblance. Both load response curves exhibit an initial increase in stress with displacement, indicating the elastic response of the soil. This is followed by a stabilization phase where the stress gradually levels off, showing that the soil approaches a plastic deformation state.

Figure 5.5 compares the vertical displacement versus stress plots obtained from two (2) small-scale physical tests (Test 2 and Test 3) and the numerical analysis performed on the slope with $\beta = 30^{\circ}$ and $D_R = 40\%$.

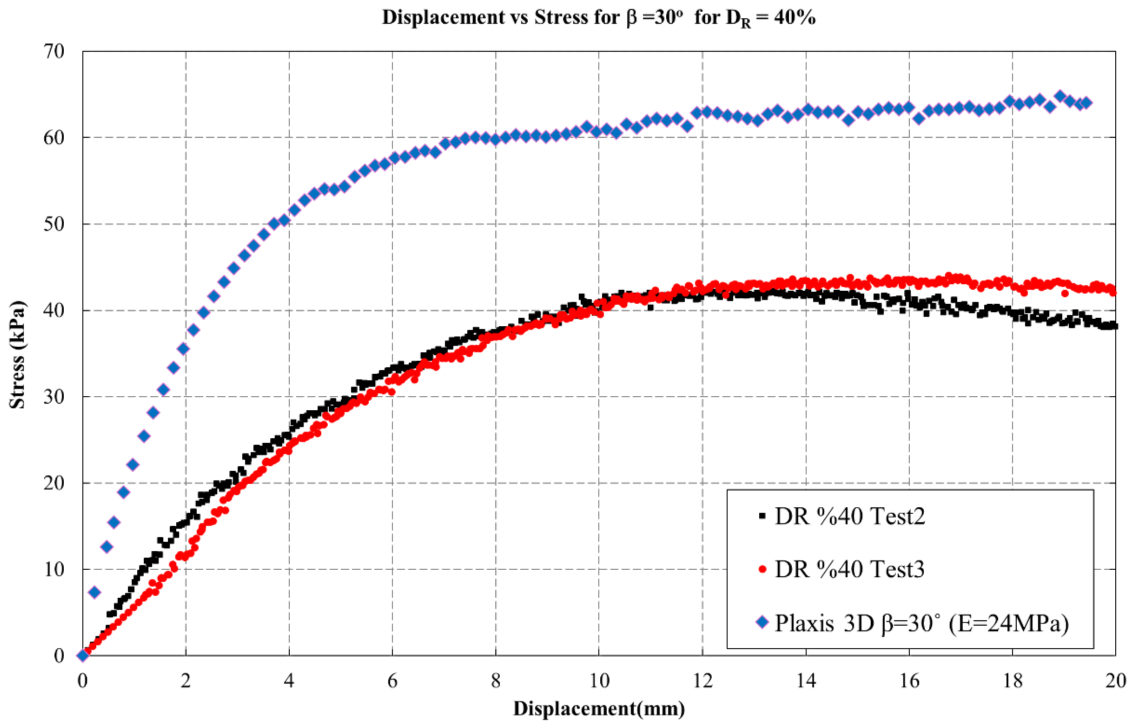

Figure 5.5. Comparison of experimental and numerical analysis results obtained for locally loaded sandy slope with $\beta = 30^{\circ}$and $D_R = 40\%$.

The Plaxis 3D results show a steeper initial stress increase, indicating higher stiffness compared to the physical tests. However, the stress levels stabilize at approximately 65 kPa corresponding to a displacement of 11 mm. The physical tests display similar patterns to each other and a response that is less stiff compared with the numerical result. The stress in both of the experiments gradually increased until plateauing at about 45 kPa after 11 mm displacement

The last comparison of experimental and numerical results was performed for the sandy slope stabilized with piles. Figure 5.6 illustrates the comparison between vertical displacement and stress plot of the locally loaded pile-stabilized stabilized slope with $\beta=30^{\circ}$ and $D_R=40\%$, obtained from model test and numerical analysis results. The analysis of the Plaxis 3D model predicted again a much steeper initial stress rise, in essence a much stiffer response compared with the actual experimental measurements. After a displacement of 20 mm the curve obtained from the numerical analysis reaches approximately 85 kPa. On the other hand, experimental results indicate a much more gradual stress increase, with the maximum value of about 70 kPa at 20 mm displacement.

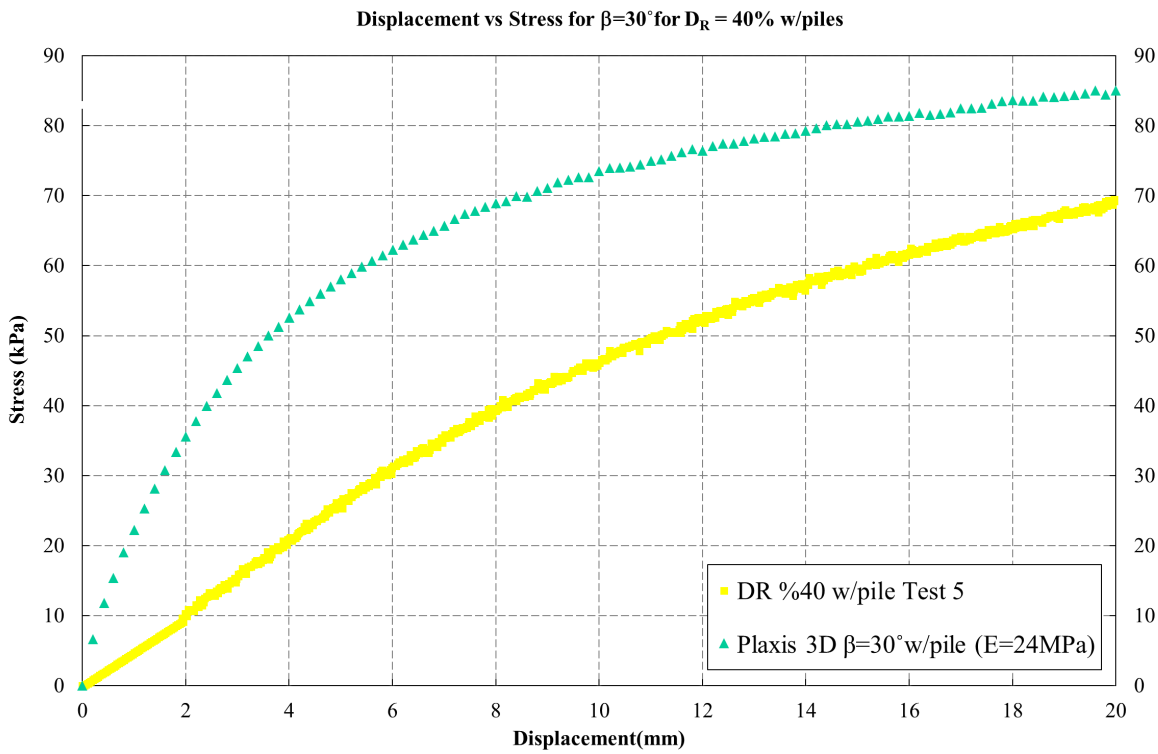

Figure 5.6. Comparison of experimental and numerical analysis results obtained for locally loaded sandy slope stabilized with piles with β = 30˚and D_R = 40%.

Overall trends observed in the results of the experiments conducted using the physical model tests were consistent with the results obtained from the analysis of the Plaxis 3D numerical model. Even though the overall behavior obtained from the numerical analysis and the experimental results are comparable and a generally good-match for all the cases compared (*i.e.*, level ground case, slope case and the pile-stabilized slope case) certain discrepancies were also identified. In particular the main discrepancy was related to the stress levels and hence, the initial stiffness response. The stress levels predicted by the analysis of the numerical model prepared in Plaxis 3D, were much higher for a given displacement compared to those calculated in the small-scale physical model tests performed in the laboratory. This difference can be attributed to several shortcomings of both laboratory tests and numerical models. Accounting for all of the scaling effects in the laboratory, especially in 1-g small-scale physical tests is not easy. This is a disadvantage of 1-g small-scale tests, and the actual stress state cannot be easily predicted or modeled accurately. An accurate stress state simulation may require the use of centrifuge tests in the laboratory. These scaling effects, and hence their effect on the in-laboratory stress development directly affect the input parameter selections in numerical simulations. Input parameters selected in the numerical analysis should be further investigated in future studies to improve the representation of small-scale stress conditions in soil to reduce discrepancies between experimental and numerical results.

6. CONCLUSIONS

The primary objective of this study was to develop a sustainable experimental setup for small-scale physical models, replicating the behavior of full-scale locally loaded sandy slopes and locally loaded sandy slope stabilized with piles. The prototype problem was defined to mimic a realistic field scenario and subsequently scaled to develop a small-scale physical model. Following the methods proposed in the literature, a small-scale physical model was constructed in the laboratory using a scale factor of 1/40 to ensure ease of application and practical feasibility. The sand selected to be used in the model tests were characterized though a series of laboratory tests, and its strength parameters were also evaluated. After the development of the experimental setup, special attention was given to controlling D_R of the sand in the model tank. Pluviation equipment was calibrated for this study, and local loading was applied using a loading plate with a hydraulic jack in a displacement-controlled manner at a rate of 0.1 mm/s. Several small-scale physical model tests were conducted on cases with locally loaded sand, locally loaded slopes and locally loaded slopes stabilized with piles. Vertical displacement and vertical stress of the loading plate were measured, and photographs of the test setup were captured continuously. In order to compare the experimental results with the numerical analysis, a 3D model of the laboratory tests was developed using finite element method (FEM)-based Plaxis 3D and hardening soil (HS) model was utilized for soils. The numerical analysis results were compared with those obtained from the experimental test results.

Based on the observations throughout the development of the experimental setup, the results of the small-scale physical model tests and numerical studies, the following conclusions were drawn.

- A well-defined scale factor and scaling method are essential when designing a small-scale physical model under 1-g conditions, as emphasized by this research.
- The pluviation calibration results demonstrated that both sand raining density and pluviation height are critical parameters in achieving the desired relative density (D_R)

within the model tank. Notably, a higher pluviation height resulted in greater density due to improved particle orientation, whereas increased sand flow rates during filling led to lower density, as there was insufficient time for the particles to orient into denser configurations.

- An initial laboratory test was conducted on level ground sand ($\beta = 0^{\circ}$) to enhance understanding of the load–settlement response of sand prepared with D_R= 40% (medium dense sand). The subgrade reaction modulus (*k*) value was calculated as 7,132 kN/m^2/m. The obtained value falls within the range for loose sands (Bowles, 1996) but is lower than that for the range provided for medium dense sands. All in all, D_R = 40% is close to the lower boundary between medium dense sand and loose sand. This slight discrepancy could have resulted from several factors but could be mainly attributed to the small plate size (0.125 m × 0.25 m) in this research study. Subgrade reaction modulus, *k*, is a parameter that depends on the loaded area. Plate size affects the results (Briaud, 2007), and for very-small plate sizes, such as the one used in this experimental program, the reliability of the results for estimating *k* is low (Teodoru and Toma, 2009). Deviations from field practice of this test in the laboratory and the use of a nearly pure sand further influenced the results. All these factors warrant further investigation.
- The vertical displacement-stress curve of the test conducted on level ground sand slope angle (β) = 0˚ with D_R 40% shows a steady increase, reflecting the increasing resistance of soil under the applied load. As stress increases, with the increase in displacements, the slope of the curve begins to decline slightly, indicating a shift into a nonlinear phase characterized by plastic behavior.
- Two (2) identical laboratory tests were conducted in the physical model tank with a β = 30˚ and D_R= 40%, to check the consistency of the desired D_R of sand, to check the repeatability of the measurements and the reliability of the experimental setup. The results stated that initially, the soil behaves linearly under small strains, but as the strain increases, it begins to deform without showing resistance. This characteristic of the response was observed in both test results. The experimental setup was deemed reliable based on the consistent results obtained for two (2) identical tests. Due to the effect of the slope and reduced bearing resistance of soils, the tests conducted at β = 30˚ show

significantly higher displacements compared to the level ground case ($\beta = 0^\circ$) under the same stress levels.

- To see the effects of D_R, additional two (2) tests were conducted with $\beta = 30^\circ$ using sandy slopes prepared at $D_R = 40\%$ and $D_R = 70\%$, representing medium-dense and dense sand cases, respectively. Slopes with $D_R = 70\%$ exhibited a steeper initial curve in the vertical displacement versus vertical stress plots compared to those with $D_R = 40\%$. As anticipated, the test with $D_R = 70\%$ showed a higher peak stress than the test with $D_R = 40\%$. In contrast, the test with $D_R = 40\%$ displayed a more gradual increase in stress without a distinct peak, indicating more of a contractive behavior under similar loading conditions. Beyond the peak stresses as the displacements increased, the vertical stress calculated in the $D_R = 70\%$ case, decreased and eventually merged with the $D_R = 40\%$ curve. This type of behavior resembles the strain-stress plots obtained during the shearing of dilative and contractive sand specimens during triaxial testing.
- To examine the effect of pile on the stability of a locally loaded sandy slope, an additional test was performed on a slope with $\beta = 30^\circ$ and $D_R = 40\%$, stabilized with piles. The initial slope of the vertical displacement-vertical stress curve of the testing showed minimal change compared with the natural slope with $\beta = 30^\circ$, that was not stabilized with piles. However, pile stabilization significantly enhanced the vertical stress response at the same vertical displacement for this slope constructed with medium-dense sand. Photographs taken post-loading revealed evidence of the arching effect, with noticeable pile-head displacements but minimal soil movement between the piles. Additionally, the central pile in the pile row exhibited the maximum horizontal displacement, while the outermost two (2) piles showed the least displacement.

For validation purposes, the experimental results from the physical model tests were compared with the results from the numerical analysis of the physical model. While the overall behavior of the vertical displacement versus stress results obtained from the numerical analysis aligned with the experimental results obtained from the small-scale models, some discrepancies were observed. Specifically, the Plaxis 3D simulations generally predicted higher stress levels for a given displacement. This was mainly attributed to the scaling effects and discrepancies in stress simulations in 1-g small-scale physical model tests. The in-laboratory stress development directly affects the input parameter selections in numerical simulations. The selection of the input parameters used in the numerical analysis should be further examined and refined to better represent the model conditions. In conclusion, this research study developed a small-scale physical model test setup that could be used for loaded slopes and slopes stabilized with piles. The numerical analysis results exhibited a load response behavior that aligned with the experimental observations. The differences observed between the experimental and numerical results were primarily attributed to the stress state simulation limitations of 1-g small-scale physical model tests. Future studies could focus on exploring the effects of varying pile configurations. The arching effect observed in pile groups could be further studied by experimenting with varying pile spacings and pile location arrangements along the slope to optimize stabilization strategies by using advanced measurement techniques, such as digital image processing.

REFERENCES

Abdelhalim, R. A., El Sawwaf, M., Nasr, A. M., Farouk, A., 2020, Experimental and numerical studies of laterally loaded piles located near oil-contaminated sand slope, *Engineering Science and Technology, an International Journal*, Vol. 23, No. 4, pp. 744-757.

Abdollahi, M., Bolouri Bazaz, J., 2017, Reconstitution of sand specimens using a rainer system, *International Journal of Engineering*, Vol. 30, No. 10, pp. 1451-1463.

Al Heib, M., Emeriault, F., Nghiem, H. L., 2020, On the use of 1g physical models for ground movements and soil-structure interaction problems, *Journal of Rock Mechanics and Geotechnical Engineering*, Vol. 12, No. 1, pp. 197-211.

Altaee, A., Fellenius, B. H., 1994, Physical modeling in sand, *Canadian Geotechnical Journal*, Vol. 31, No. 3, pp. 420-431.

American Society for Testing and Materials, 2016, *Standard Test Methods for Minimum Index Density and Unit Weight of Soils and Calculation of Relative Density* (ASTM D4254-16), West Conshohocken, PA, USA, ASTM International.

American Society for Testing and Materials, 2019, *Standard Test Methods for Maximum Index Density and Unit Weight of Soils Using a Vibratory Table* (ASTM D4253-16e1), West Conshohocken, PA, USA, ASTM International.

American Society for Testing and Materials, 2021, *Standard Test Methods for Particle-Size Distribution (Gradation) of Soils Using Sieve Analysis* (ASTM D6913/D6913M-17), West Conshohocken, PA, USA, ASTM International.

American Society for Testing and Materials, 2022, *Standard Test Method for Density (Relative Density) of Solid Pitch (Pycnometer Method)* (ASTM D2320-98(2022)e1), West Conshohocken, PA, USA, ASTM International.

American Society for Testing and Materials, 2023, *Standard Test Method for Direct Shear Test of Soils Under Consolidated Drained Conditions* (ASTM D3080/D3080M-23), West Conshohocken, PA, USA, ASTM International.

Bhattacharya, S., Lombardi, D., Dihoru, L., Dietz, M. S., Crewe, A. J., Taylor, C. A., 2012, Model container design for soil-structure interaction studies, Role of Seismic Testing Facilities in Performance-Based Earthquake Engineering: SERIES Workshop, Dordrecht, Netherlands, Springer Netherlands, pp. 135-158.

Bolton, M. D., 1986, The strength and dilatancy of sands, *Geotechnique*, Vol. 36, No. 1, pp. 65-78.

Bowles, J. E., Guo, Y., 1996, *Foundation Analysis and Design*, New York, NY, USA, McGraw-Hill.

Briaud, J.-L., 2007, Spread footings in sand: Load settlement curve approach, *Journal of Geotechnical and Geoenvironmental Engineering*, Vol. 133, No. 8, pp. 905-920.

Brinkgreve, R. B. J., Engin, E., Engin, H., 2010, Validation of empirical formulas to derive model parameters for sands, *Proceedings of 7th European Conference Numerical Methods in Geotechnical Engineering*, Trondheim, Norway.

Brinkgreve, R. B. J., Kumarswamy, S., Swolfs, W. M., Fonseca, F., Manoj, N. R., Zampich, L., Zalamea, N., 2021, PLAXIS 3D 2021 Manual, Delft, Netherlands, PLAXIS bv.

Chakraborty, T., Salgado, R., 2010, Dilatancy and shear strength of sand at low confining pressures, *Journal of Geotechnical and Geoenvironmental Engineering*, Vol. 136, No. 3, pp. 527-532.

Craig, R. F., 2004, *Craig's Soil Mechanics*, Boca Raton, FL, USA, CRC Press.

Duncan, J. M., 1996, State of the art: Limit equilibrium and finite-element analysis of slopes, *Journal of Geotechnical Engineering*, Vol. 122, No. 7, pp. 577-596.

El Sawwaf, M. A., 2005, Strip footing behavior on pile and sheet pile-stabilized sand slope, *Journal of Geotechnical and Geoenvironmental Engineering*, Vol. 131, No. 6, pp. 705-715.

Fu, Z., Jiang, G., Yuan, S., Li, A., 2019, Lateral behavior of piled bridge foundation and stabilizing piles on steep slope, *KSCE Journal of Civil Engineering*, Vol. 23, No. 10, pp. 4223-4236.

He, C., Hu, X., Liu, D., Xu, C., Wu, S., Wang, X., Zhang, H., 2020, Model tests of the evolutionary process and failure mechanism of a pile-reinforced landslide under two different reservoir conditions, *Engineering Geology*, Vol. 277, pp. 105811.

Hudson, W. R., Siddiqi, Q. S., 1970, Experimental evaluation of subgrade modulus and its application in model slab studies, Austin, TX, USA, University of Texas at Austin, Center for Highway Research.

Iai, S., 1989, Similitude for shaking table tests on soil-structure-fluid model in 1g gravitational field, *Soils and Foundations*, Vol. 29, No. 1, pp. 105-118.

Kahyaoğlu, M. R., 2010, A modeling study for load transfer mechanisms of slope stabilizing piles, Doctoral dissertation, Dokuz Eylul Universitesi.

Khati, B. S., Sawant, V. A., 2021, Experimental study of laterally loaded pile group in square arrangement near sloping ground, *International Journal of Geomechanics*, Vol. 21, No. 2, pp. 04020257.

Li, M., Zhang, L., 2022, A new sand raining technique to reconstitute large sand specimens, *Journal of Materials and Building Materials*, Vol. 12, No. 4, pp. 228-239.

Madhumathi, R. K., Ilamparuthi, K., 2018, Laboratory study on response of single pile adjacent to supported cut, *Geotechnical and Geological Engineering*, Vol. 36, pp. 3111-3133.

Mamedov, R., 2024, Study of pile configuration for efficient stabilization of clayey slopes using three-dimensional numerical analysis, MSc Thesis, Bogazici University.

Mazaheri, A. R., Paknahad, M., Nasiri, M., Hajiazizi, M., 2021, Limit analysis, numerical, and physical modeling of pile stabilized slopes using image processing analyses, *Iranian Journal of Science and Technology, Transactions of Civil Engineering*, Vol. 45, pp. 891-900.

Muthukkumaran, K., Almas Begum, N., 2015, Experimental investigation of single model pile subjected to lateral load in sloping ground, *Geotechnical and Geological Engineering*, Vol. 33, pp. 935-946.

Ozkahriman, F., & Wartman, J. Investigation of 1-g similitude laws by" modeling-of-models". Drexel University. Department of Civil, Architectural, and Environmental Engineering. Faculty Research and Publications.

Raja, N., Muthukkumaran, K., 2021, Effect of rock-socketing on laterally loaded piles installed in the proximity of sloping ground, *International Journal of Geomechanics*, Vol. 21, No. 2, pp. 04020252.

Rao, S. K., Nasr, A. M., 2010, Experimental and theoretical studies of vertical piles reinforced sand slopes loaded with strip footing, *Geotechnical Testing Journal*, Vol. 33, No. 5, pp. 385-396.

Rathod, D., Muthukkumaran, K., Thallak, S. G., 2019, Experimental investigation on behavior of a laterally loaded single pile located on sloping ground, *International Journal of Geomechanics*, Vol. 19, No. 5, pp. 04019021.

Santamarina, J. C., Cho, G. C., 2001, Determination of critical state parameters in sandy soils—simple procedure, *Geotechnical Testing Journal*, Vol. 24, No. 2, pp. 185-192.

Sharafi, H., Sojoudi, Y., 2016, Experimental and numerical study of pile-stabilized slopes under surface load conditions, *International Journal of Civil Engineering*, Vol. 14, pp. 221-232.

Stanier, S. A., Blaber, J., Take, W. A., White, D. J., 2016, Improved image-based deformation measurement for geotechnical applications, *Canadian Geotechnical Journal*, Vol. 53, No. 5, pp. 727-739.

Tekdemir, E., 2023, Three-dimensional short-term stability analysis of clayey slopes stabilized with piles, MSc Thesis, Bogazici University.

Teodoru, I. B., Toma, I. O., 2009, Numerical analyses of plate loading test, *Buletinul Institutului Politehnic din Iasi, Sectia Constructii, Arhitectura*, Vol. 55, No. 1, pp. 57.

White, D. J., Take, W. A., Bolton, M. D., 2003, Soil deformation measurement using particle image velocimetry (PIV) and photogrammetry, *Geotechnique,* Vol. 53, No. 7, pp. 619-631.

Wu, J., Kouretzis, G., Pineda, J., Suwal, L., Gibson, R., Goodwin, M., 2022, Automatic air pluviation system for physical modelling applications, *International Journal of Physical Modelling in Geotechnics*, Vol. 22, No. 5, pp. 242-259.

Wood, D. M., Crewe, A., Taylor, C., 2002, Shaking table testing of geotechnical models, *International Journal of Physical Modelling in Geotechnics*, Vol. 2, No. 1, pp. 01-13.